Five and three quantum dot systems as apparatuses for measuring energy levels

Tetsufumi Tanamoto*
Department of Information and Electronic Engineering, Teikyo University, Toyosatodai, Utsunomiya 320-8511, Japan

Tomosuke Aono
Department of Electrical and Electronic Systems Engineering, Faculty of Engineering, Ibaraki University, Hitachi 316-8511, Japan

(Received 2 April 2022; revised 1 August 2022; accepted 18 August 2022; published 1 September 2022)

A quantum dot (QD) system provides various quantum physics of nanostructures. So far, many types of semiconductor QD structures have been fabricated and investigated experimentally and analyzed theoretically. Presently, QD systems have attracted considerable attention as units for the qubit system of quantum computers. Therefore, it is vital to integrate QD systems as measurement devices in addition to qubits. Here, we theoretically investigate the side-QD system as a measurement apparatus for energy levels of the target QDs. We formulate the transport properties of both three and five QDs based on the Green's function method. The effects of the energy difference of two side-QDs on the measurement current are calculated. The tradeoff between the strength of the measurement and the back-action induced by the measurement is discussed. It is found that the medium coupling strength of the three QDs is appropriate for reading out the difference of the two energy levels.

DOI: 10.1103/PhysRevB.106.125401

I. INTRODUCTION

Quantum dot (QD) systems have been providing various topics in quantum physics for electronic systems. The interference between QDs and channel electrons is an important phenomenon that characterizes the transport properties of the system. The great developments of semiconductor nanofabrication processes enable experimentalists to directly observe the nanoworld by using the abundant technologies of the miniaturization of semiconductor devices. Numerous excellent experimental works have been carried out in this mesoscopic field [1–10]. Recently, many QD systems have become a target structure of spin qubits because spin qubits enter into their development phase with many QDs [11–14]. Thus, the transport properties of many QDs are of newfound interest in several fields of physics and engineering.

In QD systems, the changes in energy levels of QDs to external controls are very small, and detecting energy levels is very difficult [15–19]. Generally speaking, we can obtain the knowledge of the energy levels indirectly through the current line attached close to the target QDs. In addition, we have to consider the effect of the back-action by the measurements. In order to obtain strong signals, the coupling between the target structure and the measurement structure should be large. However, the strong coupling to the target structure tends to destroy the coherence of the system. The tradeoff between the measurement and the back-action is an important issue.

In this study, we theoretically describe how to measure the difference between the energy levels of two QDs by using the side-QDs system. We focus on the measurement of the QDs in the side-QD system, as shown in Fig. 1. In the conventional side-QD structure [Fig. 1(a)], the arrangement of QDs is symmetric to the center current line [S3-QD3-D3 in Fig. 1(a)], therefore, we cannot judge which of the QDs has a higher energy level when we measure only the current of the structure in Fig. 1(a). However, we can distinguish the two QDs by adding two other current lines, as shown in Fig. 1(b). For distinguishing the two energy levels, it is sufficient to compare the currents separately. For example, by switching on the current line 1 while the other two current lines are switched off, the current line 1 reflects only the energy levels of the QD2. By combining this with the case where only the current line 3 is switched on, we will be able to judge which of the QD2 and QD4 has a higher energy level. Similarly, we can use the case where the current line 5 is switched on while the other two currents are switched off. On the other hand, when the three currents flow at the same time, we can consider an interesting process that does not appear for the separate current detection. When the three current lines are simultaneously switched on, new current passes are generated from the source Si to the drain Dj ($i \neq j$) through the QD between the two current lines. It is expected that these passes enhance both the measurement and the back-action. We numerically calculate the transport properties of Figs. 1(a) and 1(b), and discuss the tradeoff of the coupling strength and the back-action. Hereafter, we call Figs. 1(a) and 1(b) as the "three-QD" and "five-QD" cases, respectively.

The side-QD structures have been mainly investigated as the typical setup for observing the Fano effect, in which the current shows a dip via the interference between the energy level of the QD and the channel current [5–10,20–26]. Moreover, the side-QD structures with two QDs have been called the two-impurity Kondo effects. In the early research, the energy levels of the two QDs were the same [27–30], and recently the difference of the two energy levels is treated to

*tanamoto@ics.teikyo-u.ac.jp

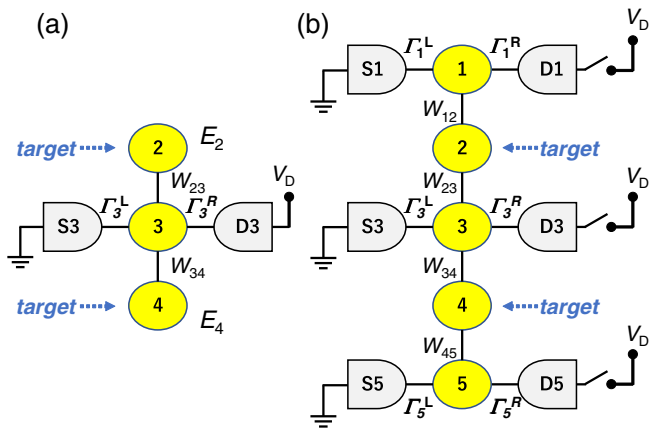

FIG. 1. Quantum dot (QD) system considered in this study. In each figure, the center circles show the QDs, and the voltages are applied between the sources Si and the drains Di ($i = 1, 3, 5$). (a) Three QDs system, which includes two side QDs and one current line. (b) Five QDs system, which includes the three current lines. Γ_i^α and W_{ij} are the tunneling couplings between the electrodes ($\alpha = L, R$) and the QDs and those between two QDs, respectively ($i = 1, 3, 5$, $j = 2, 4$) [see also Eqs. (1) and (2) in the main text]. This study targets the detection of the energy levels of QD2 and QD4. The right-hand sides of the current lines in (b) can be switched on and off to select the currents. By choosing the current lines, the relative energy level between QD2 and QD4 can be detected.

be more widely. In [31], the resonant tunneling effect through the two impurity energy levels was discussed, and it was found that a significantly narrowed peak structure superimposes over a broad peak structure because of the coupling between the energy levels and the electrode. In addition, the conductance is sensitively affected by the difference in the impurity energy levels. These results are analogous to the Dicke effect in quantum optics [32], where fast and slow relaxation modes appear owing to the interaction between the coupled relaxation channels. Similar effects have been extensively discussed for electrical conduction in mesoscopic systems [33]. In two-side QD systems, the Dicke-type effect has been discussed in terms of the Kondo effect [34–39].

The structure of many QDs with many current lines will be required in the integration of the semiconductor qubits. This is because packing qubits and the detection current line into a small area will be important to maintain the decoherence time of the system. The detection of the energy difference between the two QDs is required in many cases of quantum computing systems. The first example is the detection of the gradient magnetic fields [26,40,41], which is important to control the qubits individually. When the magnetic fields change depending on the position of the QDs, the Zeeman energy levels change accordingly. It is expected that experimentalists can infer the magnitude of the energy difference of the QDs by measuring the transport properties. Then, the side-QD system could be implemented to estimate the energy differences as a candidate of the measurement system. The second example is the detection of two qubits in the FinFET(Fin Field Effect Transistor) structure [42,43]. In [43], QDs embedded between the channel of the FINFET work as the qubits. The results of the final qubit state affect the energy levels. In the spin qubit system, it is important to detect whether the two qubits have the same spin directions (both $|\uparrow\uparrow\rangle$ or $|\downarrow\downarrow\rangle$) or opposite spin directions ($|\uparrow\downarrow\rangle$ or $|\downarrow\uparrow\rangle$).

This system can also be used to the third example where the electric field is applied across the vertical direction of the QDs in Fig. 1. When there is an applied voltage across the QD1-QD2-QD3-QD4-QD5 via some insulators between the QDs and the additional electrodes (not shown), we can expect the gradient changing energy levels. By this vertical electric field, the interference between the QDs and the channel electrons can be controlled, and the current reflects the different energy levels. Thus, we aim to study how the current characteristics of the channel reflect the difference of the energy levels of two QDs.

We use the Green's function methods developed by [44,45], which enable us to formulate the current characteristics. The formulation of the five QD system is very complicated and, therefore, it is better to observe the characteristics of the system without the Kondo effect. Moreover, it seems that it is not easy to experimentally observe the two-channel Kondo [46,47]. In this study, we neglect the Kondo effect and onsite Coulomb interaction in each QD.

The rest of this study is organized as follows. In Sec. II, we show our formalism using the standard Green's function method. In Sec. III, we explain our measurement setup. In Sec. IV, we show the numerical results of our method. In Sec. V, we discuss our results. In Sec. VI, we summarize and conclude this study.

II. GREEN'S FUNCTION METHODS

We investigate the transport properties of both the three and five QD systems depicted in Fig. 1. The formulation of the three QD systems is the case $W_{12} = 0 = W_{45}$ of the five QD system. Thus, we derive the formula of the five QD system. The Hamiltonian of the five QD system is given by

$$\begin{aligned} H = &\sum_s \sum_{i=1}^{5} E_i d_{is}^\dagger d_{is} + \sum_s \sum_{i=1,3,5} \sum_{\alpha=L,R} \sum_{k_\alpha} E_{k_\alpha} c_{ik_\alpha,s}^\dagger c_{ik_\alpha,s} \\ &+ \sum_s \sum_{i=1,3,5} \sum_{\alpha=L,R} \sum_{k_\alpha} \left[V_{k_\alpha,s,i} c_{ik_\alpha,s}^\dagger d_{is} + V_{k_\alpha,s,i}^* d_{is}^\dagger c_{ik_\alpha,s} \right] \\ &+ \sum_{i=1}^{4} \sum_s W_{i,i+1} (d_{is}^\dagger d_{i+1,s} + \text{H.c.}), \end{aligned} \tag{1}$$

where $c_{iks}^\dagger$ (c_{iks}) creates (annihilates) an electron with momentum k and spin s in the i leads ($i = 1, 3, 5$), and $d_{is}^\dagger$ (d_{is}) creates (annihilates) an electron in the QDs ($i = 1, \ldots, 5$). We assume that there is one energy level in each QD. The coupling coefficients of the leads to the QDs are given by

$$\Gamma_{is}^\alpha(\omega) = 2\pi \sum_{k_\alpha} |V_{k_\alpha,s,i}|^2 \delta(\omega - E_{k_\alpha}). \tag{2}$$

We also assume that $\Gamma_i^\alpha(\omega) \equiv \Gamma_{i\uparrow}^\alpha(\omega) = \Gamma_{i\downarrow}^\alpha(\omega)$.

Following [44,45], the current I_{iL} of the ith left electrode is derived from the time derivative of the number of electrons

$N_{iL} \equiv \sum_{k_L s} c^\dagger_{ik_L s} c_{ik_L s}$ by the left electrode, given by

$$\begin{aligned} I_{iL}(t) &= -e\left\langle \frac{dN_{iL}}{dt} \right\rangle = -\frac{ie}{\hbar}\langle [H, N_{iL}] \rangle, \\ &= \frac{ie}{\hbar} \sum_{k_L, s} \left[V_{k_L s, i} \langle c^\dagger_{ik_L s} d_{is} \rangle - V_{k_L s, i} \langle d^\dagger_{is} c_{ik_L s} \rangle \right] \\ &= \frac{2e}{\hbar} \mathrm{Re} \left\{ \sum_{k_L, s} V_{k_L s, i} G^<_{d_{is}, c_{ik_L s}}(t, t) \right\} \\ &= \frac{2e}{\hbar} \int dE \, \mathrm{Re} \left\{ \sum_{k_L, s} V_{k_L s, i} G^<_{d_{is}, c_{ik_L s}}(E) \right\}, \end{aligned} \tag{3}$$

where

$$G^<_{d_{is}, c_{ik_\alpha s}}(t, t') \equiv i \langle c^\dagger_{ik_\alpha s}(t') d_{is}(t) \rangle, \tag{4}$$

$$G^<_{c_{ik_\alpha s}, d_{is}}(t, t') \equiv i \langle d^\dagger_{is}(t') c_{ik_\alpha s}(t) \rangle, \tag{5}$$

and

$$G^<_{c_{ik_\alpha s}, d_{is}}(t, t) = -\left[G^<_{d_{is}, c_{ik_\alpha s}}(t, t) \right]^*. \tag{6}$$

We assume that the total current is conserved between the source (left electrode) and drain (right electrode) which means that the left-electrode currents I_{iL} and the right-electrode currents I_{iR} $(i = 1, 3, 5)$ satisfy the relation $I_L = -I_R$ where $I_\alpha = \sum_{i=1,3,5} I_{i\alpha}$ for $\alpha = L, R$. Then, we can express the current through the device by $I = (I_L + I_L)/2 = (I_L - I_R)/2 = \sum_{i=1,3,5}(I_{iL} - I_{iR})/2$. Hereafter, we also assume that the spin-flip process is neglected, and the suffix s is omitted.

The Green's functions are derived using the equation of motion method [45]. For example, the time-dependent behavior of the operator $d_i(t)$ is derived from $i\hbar \frac{d\, d_i(t)}{dt} = [H, d_i(t)]$, and we have

$$\omega d_i(\omega) = [H, d_i(\omega)]. \tag{7}$$

As shown in the Appendix C and D, by combining various pairs of the operators, all Green's functions are obtained.

The Green's functions of the electrodes $(\alpha = L, R)$ are the free-particle Green's functions given by

$$g^<_\alpha(k, \omega) = 2\pi i f\left(E_{k_\alpha}\right) \delta\left(\omega - E_{k_\alpha}\right), \tag{8}$$

$$g^>_\alpha(k, \omega) = 2\pi i \left[f\left(E_{k_\alpha}\right) - 1 \right] \delta\left(\omega - E_{k_\alpha}\right), \tag{9}$$

$$g^r_\alpha(k, \omega) = \frac{1}{\omega - E_{k_\alpha} + i\delta}, \tag{10}$$

where $f(\epsilon)$ is the Fermi distribution function. We define the Fermi energy E_F as that of the source electrodes. The Green's functions of the QDs are given by

$$\begin{aligned} g^r_{di}(\omega) &= 1/\left[\omega - E_i - \Sigma^r_i(\omega) \right] \\ &= \frac{\omega - E_i - \Lambda_i(\omega) - \frac{i}{2}\Gamma_i}{[\omega - E_i - \Lambda_i(\omega)]^2 + \Gamma_i^2/4} = \frac{b_i(\omega)^*}{D_i(\omega)}, \end{aligned} \tag{11}$$

$$b_i(\omega) \equiv \omega - E_i - \Lambda_i(\omega) + i\Gamma_i/2, \tag{12}$$

$$D_i(\omega) \equiv [\omega - E_i - \Lambda_i(\omega)]^2 + \Gamma_i^2/4, \tag{13}$$

$$\Sigma^{r,a}_i(\omega) = \sum_\alpha \sum_{k_\alpha} \frac{|V_{k_\alpha, i}|^2}{\omega - E_{k_\alpha} \pm i\eta} = \Lambda_i(\omega) \mp \frac{i}{2}\Gamma_i, \tag{14}$$

$$\Gamma_i \equiv \Gamma^L_i + \Gamma^R_i, \quad \Lambda_i(\omega) \equiv \sum_\alpha \sum_{k_\alpha} \frac{|V_{k_\alpha, i}|^2}{\omega - E_{k_\alpha}}, \tag{15}$$

$$\begin{aligned} g^<_{di}(\omega) &= g^r_{di}(\omega) \Sigma^<_i(\omega) g^a_{di}(\omega) \\ &= \frac{i\left[\Gamma^L_i f_{iL}(\omega) + \Gamma^R_i f_{iR}(\omega) \right]}{[\omega - E_i - \Lambda_i(\omega)]^2 + \Gamma_i^2/4}, \end{aligned} \tag{16}$$

where $\Lambda_i(\omega)$ is assumed to be constant and included in E_i in the following. The Fermi distribution function $f_{i\alpha}(\omega)$ is given by $f_{i\alpha}(\omega) = \{\exp[(\omega - \mu_\alpha)/(k_B T)] + 1\}^{-1}$ (k_B, μ_α, and T are the Boltzmann constant, the chemical potential of the α electrode, and the temperature). After the long derivation process, the retarded and advanced Green's functions G_{dij} (r and a are omitted) are given by

$$G_{d11}(\omega) = \frac{[1 - C_{32}(\omega)][1 - C_{54}(\omega)] - C_{34}(\omega)}{\Delta_c} g_{d1}(\omega), \tag{17}$$

$$G_{d31}(\omega) = \frac{[1 - C_{54}(\omega)]}{\Delta_c} W_{12} W_{23} C_{32}(\omega) g_{d1}(\omega), \tag{18}$$

$$G_{d51}(\omega) = \frac{W_{12} W_{23} C_{32}(\omega) W_{43} W_{54} C_{54}(\omega)}{\Delta_c} g_{d1}(\omega), \tag{19}$$

$$G_{d13}(\omega) = \frac{[1 - C_{54}(\omega)]}{\Delta_c} W_{23} W_{12} C_{12}(\omega) g_{d3}(\omega), \tag{20}$$

$$G_{d33}(\omega) = \frac{[1 - C_{54}(\omega)][1 - C_{12}(\omega)]}{\Delta_c} g_{d3}(\omega), \tag{21}$$

$$G_{d53}(\omega) = \frac{[1 - C_{12}(\omega)]}{\Delta_c} W_{43} W_{54} C_{54}(\omega) g_{d3}(\omega), \tag{22}$$

$$G_{d15}(\omega) = \frac{W_{45} W_{34} C_{34}(\omega) W_{23} W_{12} C_{12}(\omega)}{\Delta_c} g_{d5}(\omega), \tag{23}$$

$$G_{d35}(\omega) = \frac{W_{45} W_{34} C_{34} [1 - C_{12}(\omega)]}{\Delta_c} g_{d5}(\omega), \tag{24}$$

$$G_{d55}(\omega) = \frac{[1 - C_{34}(\omega)][1 - C_{12}(\omega)] - C_{32}(\omega)}{\Delta_c} g_{d5}(\omega), \tag{25}$$

where

$$C_{ij} \equiv |W_{ij}|^2 g_{di} g_{dj}, \tag{26}$$

$$\Delta_c \equiv [1 - C_{54}](1 - C_{12} - C_{32}) - C_{34} + C_{12} C_{34}. \tag{27}$$

In addition, when three Green's functions A, B, and C have the relation of $A = BC$, the lesser Green's function $A^<$ can be derived from [44,45]

$$A^<(E) = B^r(E) C^<(E) + B^<(E) C^a(E). \tag{28}$$

The derivation of the lesser Green's functions is more complicated than that of the retarded and advanced Green's functions. After the long derivation process using Eq. (28), we have the current formula for the five QDs, given by

(see Appendix D)

$$I = \frac{e}{\hbar}\int \frac{d\omega}{2\pi}\left\{ \frac{|W_{12}W_{23}W_{34}W_{54}|^2}{\left|\Delta_c^r\right|^2}\frac{1}{D_1D_2D_3D_4D_5}F_{12345} + \frac{\left|1-C_{12}^r\right|^2}{|\Delta_c^r|^2}\frac{|W_{34}W_{54}|^2}{D_3D_4D_5}F_{345} + \frac{\left|1-C_{54}^r\right|^2}{|\Delta_c^r|^2}\frac{|W_{23}W_{12}|^2}{D_1D_2D_3}F_{123} \right.$$
$$\left. + \frac{\left|\left(1-C_{34}^r\right)\left(1-C_{12}^r\right)-C_{32}^r\right|^2}{\left|\Delta_c^r\right|^2 D_5}F_{55}(\omega) + \frac{\left|\left(1-C_{32}^r\right)\left(1-C_{54}^r\right)-C_{34}^r\right|^2}{\left|\Delta_c^r\right|^2 D_1}F_{11}(\omega) + \frac{\left|1-C_{54}^r\right|^2\left|1-C_{12}^r\right|^2}{\left|\Delta_c^r\right|^2 D_3}F_{33}(\omega)\right\}, \quad (29)$$

where F_{ii}, F_{12345}, F_{123}, and F_{345} are defined in the Appendix D. When $W_{12} = W_{45} = 0$ in Eq. (29), we have the current of the three QDs [Fig. 1(a)], given as

$$I_3 = \frac{e}{\hbar}\int \frac{d\omega}{2\pi}\frac{\Gamma_3^L\Gamma_3^R}{|1-C_{32}-C_{34}|^2 D_3}[f_{3L}(\omega) - f_{3R}(\omega)]. \quad (30)$$

The density of the states (DOS) is calculated by

$$\rho(\epsilon) = -\frac{1}{\pi}\mathrm{Im}\left[G_{d11}^r(\epsilon) + G_{d33}^r(\epsilon) + G_{d55}^r(\epsilon)\right]. \quad (31)$$

In the following, we mainly show the results of $T \to 0$ limit, where $\partial f(\epsilon)/\partial\epsilon \to -\delta(\epsilon - E_F)$.

III. CIRCUIT DETECTION

We would like to detect the difference of E_2 and E_4 by using a simple circuit. In a conventional circuit, the voltage signal is better for output than the current signal. In order to transform the current change into voltage change, the additional resistor R_D is set to the drain part of the QD system. Here, we consider a simple measurement system, as shown in Fig. 2, where Ohm's law leads to the following relation:

$$V_D = I_D R_D + V_{\mathrm{out}}. \quad (32)$$

The current I_D is the function of the V_{out}; thus, this equation should be solved self-consistently. However, by assuming that the applied voltages are low, and using $I_D = \sigma V_{\mathrm{out}}$, we have

$$V_{\mathrm{out}} = \frac{1}{1+\sigma R_D}V_D. \quad (33)$$

In order to effectively reflect the change in σ, the resistor should be in the order of σ^{-1} such that

$$R_D = 1/\sigma \sim \hbar/(2e^2). \quad (34)$$

The amplifying rate is given by

$$\frac{dV_{\mathrm{out}}}{d[E_2-E_4]} = -\frac{R_D}{(1+\sigma R_D)^2}\frac{d\sigma}{d[E_2-E_4]}V_D. \quad (35)$$

In Fig. 1(a), we take $\sigma = \sigma_3$, and in Fig. 1(b), we take $\sigma = \sum_{i=1,3,5}\sigma_i$, where σ_i is the conductance of the ith current line. The relation between the conductance σ_i and the transmission coefficient $\mathcal{T}_i$ is given by

$$\sigma_i = \frac{2e^2}{h}\mathcal{T}_i. \quad (36)$$

The shot noise is simply estimated by [48,49]

$$S = \frac{2e^2}{\pi\hbar}\sum_i \mathcal{T}_i(1-\mathcal{T}_i)|eV|, \quad (37)$$

where the sum is taken for $i = 1, 3, 5$ for the five QD case and only $i = 3$ for the three QD case, respectively. The measurement time is defined by [50]

$$t_{\mathrm{meas}}^{-1} \equiv \frac{(\Delta I)^2}{4S}, \quad (38)$$

where we take ΔI as the difference of the current from that at $E_2 = E_4$. Moreover, we exclude the region of $\Delta I = 0$ in the numerical results below. In the calculation of the noise power S, we need the concrete value for the applied voltage V_D. For $V_D = 10 \sim 100\ \mu$eV [1,2], the current I is in order of $I \sim V_D/[2R_D] \sim 0.17$–$1.7$ nA, where approximately 10–100 electrons flow per 1 ps. Here, we assume $V_D = 8\ \mu$eV. Regarding the values for the Γ, $\Gamma = 0.5\ \mu$eV is used in [1], and $\Gamma = (3\ \mathrm{ns})^{-1}$ is used in [2,3]. Here, we take $\Gamma_0 = 10\ \mu$eV as the unit of the Γ, and $E_F = 4.5\Gamma_0$. From Refs. [44,45], the QD connected to two electrodes shows the resonant tunneling behavior in which the current has a peak when the bias voltage becomes larger than the energy level of the QD. Thus, the linear approximation (33) is appropriate for $E_i > V_D$, which corresponds to the region other than the neighbor of $(E_2, E_4) = (0, 0)$ in the calculations of Sec. IV because $V_D \ll E_F$.

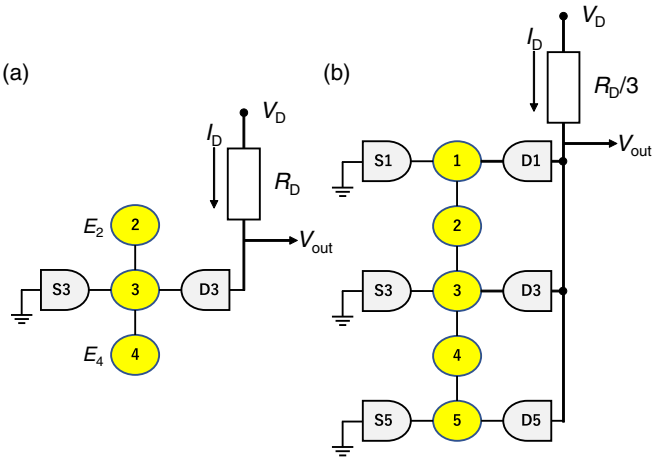

FIG. 2. Simple setup of converting the current change of the QD system into voltage change for both (a) the three QD case and (b) the five QD case. We take the resistance R_D as the same order of the QD system, such as $R_D = 25.8\ \mathrm{k}\Omega$.

Back-action

Usually, it is assumed that the energy levels of QDs are not changed. However, the energy levels of QDs are changed in several situations. For example, it can be considered that there are trap sites near the QDs, and the charge distribution of the trap site changes depending on the externally applied voltage. In addition, we can consider the case of [43,51] where the energy levels are affected by the directions of the spins that fill the lower energy levels of the same QDs. In these cases, it is natural to consider that both E_2 and E_4 are changed by the measurements. Thus, it is meaningful to analyze the effect of the measurements on those energy levels. Because the change of the energy levels affects the electronic states of electrons, it is related to the decoherence effect. In many literatures, the decoherence effects have been analyzed regarding the noise effect on the coherence. However, the detailed noise analysis of the qubits is complicated and requires a lot of experimental data [4]. Here, we consider that the decoherence in QD2 and QD4 is induced by the measurement of the currents 1, 3, and 5. That is, it is possible that electrons in QD2 or QD4 lose their coherence while they move back and forth to the channel QDs 1, 3, and 5. We simply describe the decoherence time caused by the interaction. This process can be described by the golden rule [52], where the last term of the Hamiltonian (1), $H_{\rm int}(t) \equiv \sum_{i=1}^{4}\sum_s W_{i,i+1}[d_i^\dagger(t)d_{i+1}(t) + \text{H.c.}]$, is treated as the perturbation term, and the nonperturbated terms are those of the current lines $\text{S}_i - \text{QD}_i - \text{D}_i$ $(i = 1, 3, 5)$. Then, the relaxation rate $\Gamma_{\rm relax}$ can be defined by

$$\Gamma_{\rm relax} \approx \frac{1}{\hbar^2}\int_{-\infty}^{\infty} d\tau\, e^{-i\omega_{01}\tau}\langle H_{\rm int}(\tau)H_{\rm int}(0)\rangle, \tag{39}$$

where $\omega_{01} = |E_2 - E_4|$. The decoherence time $t_{\rm dec}$ is defined by $t_{\rm dec} \equiv \Gamma_{\rm relax}^{-1}$. The final form of $t_{\rm dec}$ is given by (see Appendix A)

$$\begin{aligned}
t_{\rm dec}^{-1} \approx& \sum_i \frac{|W_{i,i+1}|^2}{\hbar^2}\int\frac{d\epsilon'}{2\pi}[g_{di}^{<}(\epsilon'+\omega_{01})g_{di+1}^{>}(\epsilon') + g_{di+1}^{<}(\epsilon'+\omega_{01})g_{di}^{>}(\epsilon')] \\
=& [1-f(E_2)]\left(\frac{|W_{12}|^2}{\hbar^2}\frac{\Gamma_1^L f_L(E_2+\omega_{01}) + \Gamma_1^R f_R(E_2+\omega_{01})}{[E_2+\omega_{01}-E_1-\Lambda_1(E_2+\omega_{01})]^2+\Gamma_1^2/4} + (1\to 3)\right) \\
&+ f(E_2)\left(\frac{|W_{12}|^2}{\hbar^2}\frac{\Gamma_1^L[1-f_L(E_2-\omega_{01})] + \Gamma_1^R[1-f_R(E_2-\omega_{01})]}{[E_2-\omega_{01}-E_1-\Lambda_1(E_2-\omega_{01})]^2+\Gamma_1^2/4} + (1\to 3)\right) \\
&+ [1-f(E_4)]\left(\frac{|W_{43}|^2}{\hbar^2}\frac{\Gamma_3^L f_L(E_4+\omega_{01}) + \Gamma_3^R f_R(E_4+\omega_{01})}{[E_4+\omega_{01}-E_3-\Lambda_3(E_4+\omega_{01})]^2+\Gamma_3^2/4} + (3\to 5)\right) \\
&+ f(E_4)\left(\frac{|W_{43}|^2}{\hbar^2}\frac{\Gamma_3^L[1-f_L(E_4-\omega_{01})] + \Gamma_3^R[1-f_R(E_4-\omega_{01})]}{[E_4-\omega_{01}-E_3-\Lambda_3(E_4-\omega_{01})]^2+\Gamma_3^2/4} + (3\to 5)\right).
\end{aligned} \tag{40}$$

Here, $f(E_i)$ and $1 - f(E_i)$ mean that there is an electron in the E_i level and that there is no electron in the E_i level, respectively $(i = 2, 4)$. In order to treat an average case, we take $f(E_2) = f(E_4) = \frac{1}{2}$ in the following calculations.

IV. NUMERICAL RESULTS

For simplicity, we assume the uniform case of $W_{ij}(= W)$ and $\Gamma_i(= \Gamma)$ at zero temperature $(T = 0)$. The effects of the nonuniform parameters and the finite temperature are discussed in the Appendix B. When we use QDs 1, 3, and 5, with their electrodes as the measurement structure to detect the energy levels of QD 2 and 4, the magnitude of W compared with Γ can be regarded as the strength of measurement. Thus, we can distinguish the following three regions: (1) *strong* measurement of $W > \Gamma$ (Figs. 4 and 5), (2) *medium* measurement of $W \approx \Gamma$ (Figs. 6 and 7), and (3) *weak* measurement of $W < \Gamma$ (Figs. 8 and 9).

Since we focus on the detection of the difference of the two energy levels, the change of the currents from those at $E_2 = E_4$ is important. Thus, all numerical results are described as the functions of E_2 and E_4. As explained in the Introduction, we assume that the gradient fields are generated by the applied magnetic fields or electric fields. Thus, it is appropriate that the difference of the energy levels between the adjacent QDs are assumed to be uniform such that $\delta \equiv E_2 - E_1 = E_3 - E_2 = E_4 - E_3 = E_5 - E_4$. The following graphs show the conductance and other detectable physical values, aiming that the experimentalists can estimate the difference of the energy levels of the QDs from the calculated current characteristics.

Figure 3 shows the DOS of Eq. (31) for the three coupling regions. In the strong measurement case of Figs. 3(a) and 3(d), the central peak shows the energy level of the QD2 (we fix E_2 in the calculation), and the other peaks show the coupling to the electrodes. In the medium measurement of Figs. 3(b) and 3(e), we can see both the central sharper peak and the two broader peaks, which are similar characteristics to those discussed in [34,35,37–39]. In the weak coupling cases [Figs. 3(c) and 3(f)], we observe the Fano dip structure over the broad Lorentzian structure. When the three QD medium coupling case [Fig. 3(b)] is compared with that of five QD case [Fig. 3(e)], the peak structures are broadened. This is because the five QD structure has additional electrodes compared with the three QD case, and the coupling to the electrodes makes the Lorentzian wider. In contrast, for the weak coupling case, there is no significant difference in both the three QD case and the five QD case. This is because the coupling between the channel current and the electrodes is weak, resulting in the smaller effects of the additional electrodes of

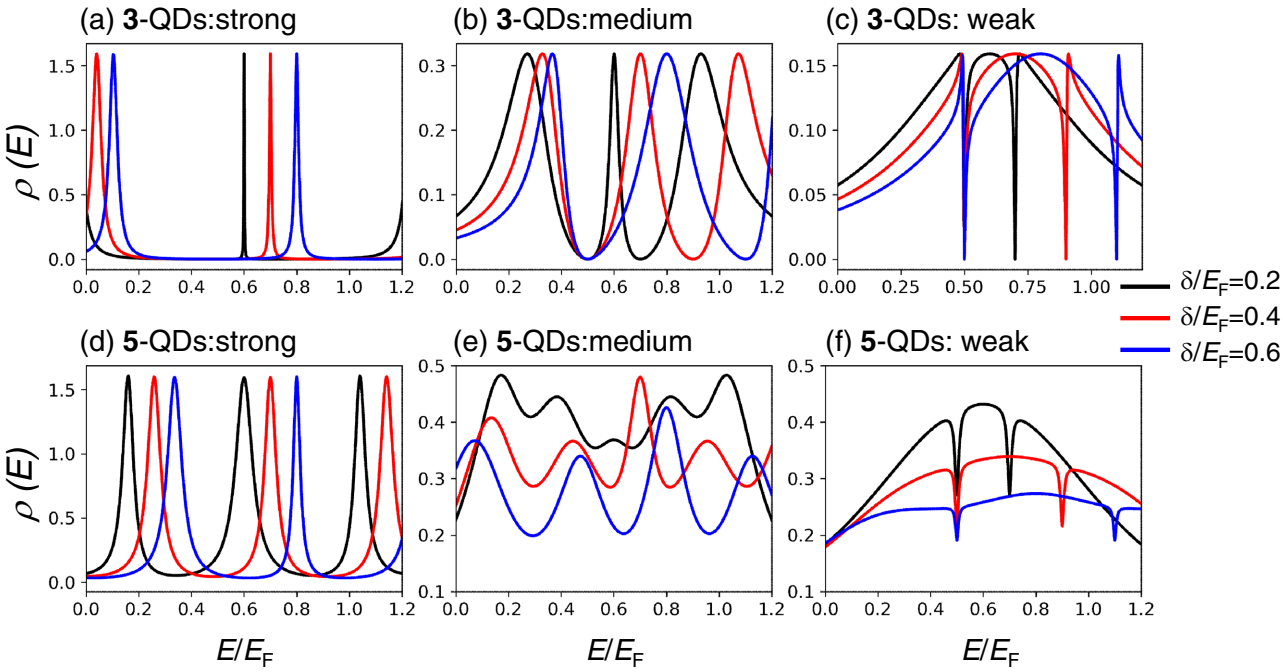

FIG. 3. The density of states (DOS), Eq. (31), for (a), (d) the strong measurement case of $\Gamma = 0.2\Gamma_0$ and $W = 2\Gamma_0$, (b), (e) the medium measurement case of $\Gamma = W = \Gamma_0$, and (c), (f) the weak measurements case of $\Gamma = 2\Gamma_0$ and $W = 0.2\Gamma_0$. $\Gamma_0 = 10$ μeV and $E_2/E_F = 0.5$. (a)–(c) For the three QD case. (d)–(f) For the five QD case.

the five QD structure. The effect of the increasing detuning $\delta = E_{i+1} - E_i$ is prominent in the case of the five QD case for the medium measurement. This is because there are two additional QDs in the case of the five QD case in Fig. 3(e).

Figure 4 shows the transport properties of the strong measurement case. We can see that the conductances have the peak structures around the Fermi energy. This can be understood by considering that the two kinds of peaks of Figs. 3(a) and 3(d) overlap around the Fermi energy. Some of the outputs

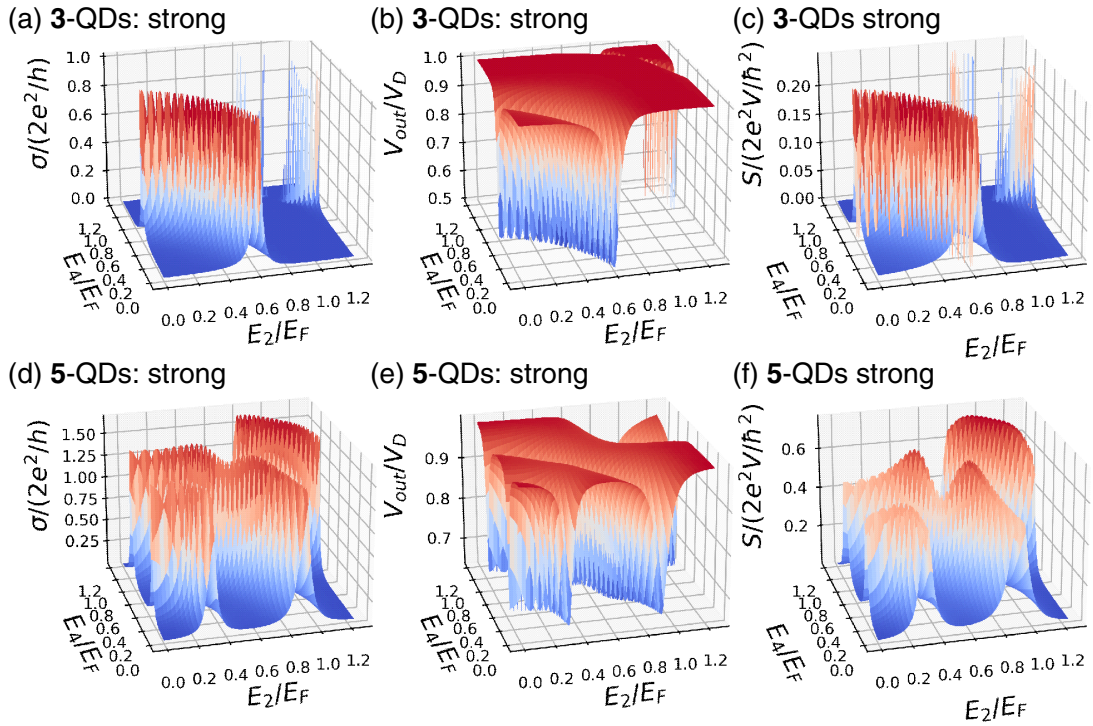

FIG. 4. The strong measurement case of $\Gamma = 0.2\Gamma_0$ and $W = 2\Gamma_0$ as functions of E_2 and E_4 for several $\delta = (E_4 - E_2)/2$. $\Gamma_0 = 10$ μeV and $V_D = 8$ μeV. (a), (d) Conductance, (b), (e) V_{out}. (c), (f) The noise power S. (a)–(c) Three QD case and (d)–(f) five QD case.

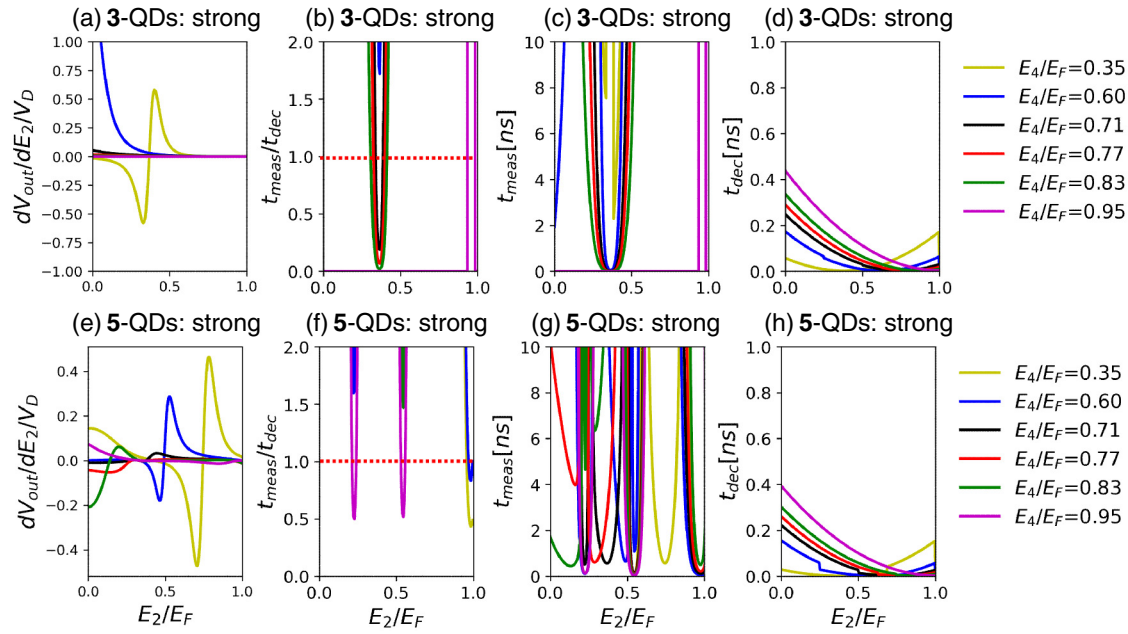

FIG. 5. The strong measurement case of $\Gamma = 0.2\Gamma_0$ and $W = 2\Gamma_0$ as functions of E_2 and E_4 for several $\delta = (E_4 - E_2)/2$. $\Gamma_0 = 10$ μeV and $V_D = 8$ μeV. (a), (e) $\frac{dV_{\rm out}}{d(E_2-E_4)}/V_D$. (b), (f) $t_{\rm meas}/t_{\rm dec}$. (c), (g) $t_{\rm meas}$. (d), (h) $t_{\rm dec}$. (a)–(d) Three QD case and (e)–(h) five QD case. The dotted lines in (b) and (f) indicate the boundary of the effective measurement $t_{\rm meas} < t_{\rm dec}$.

$V_{\rm out}$ become the half of V_D. A comparison of Figs. 4(c) and 4(f) shows that the coupling of the five QD case induces a larger noise than the three QD case. This is because of the three current lines attached to the QDs for the five QD case. In addition, owing to the fact that the coupling Γ to the electrodes is weaker than the coupling W to the QDs, the shot noises [Figs. 4(c) and 4(f)] are smaller than those of the following medium measurement case. Figures 5(c) and 5(g) show the measurement times. Here, in the calculation of $t_{\rm meas}$ [Eq. (38)], we exclude the line around $E_2 = E_4$, which results in the divergence structures in Figs. 5(b), 5(c), 5(f), and 5(g). The dot lines in Figs. 5(b) and 5(f) show the boundary lines

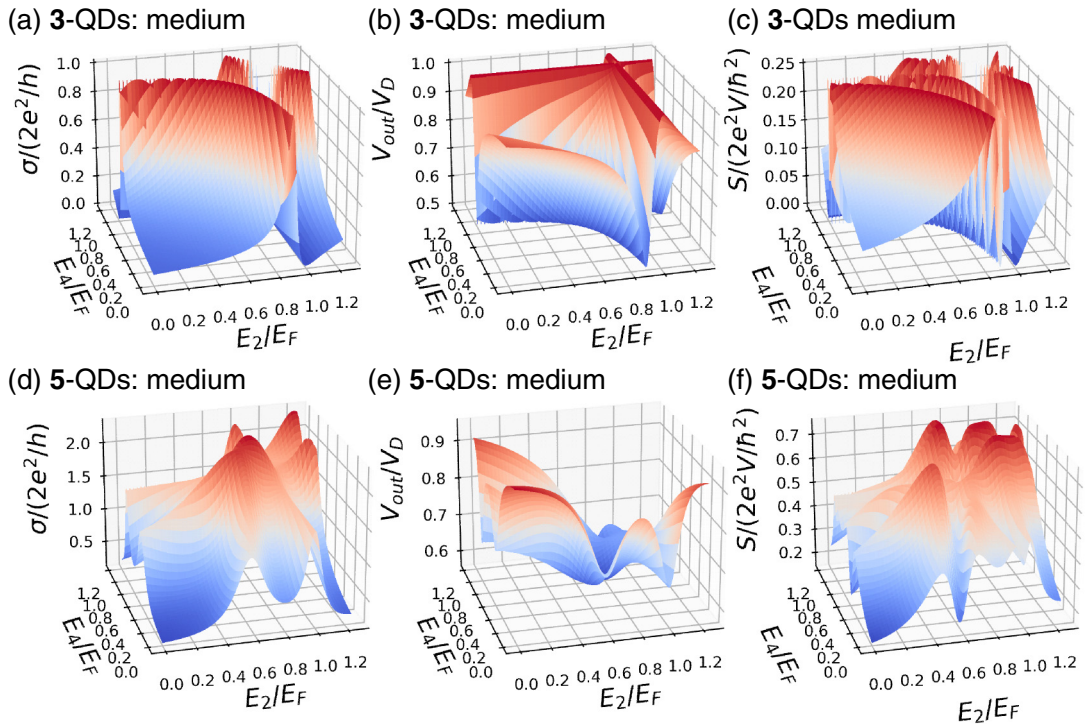

FIG. 6. The medium measurement case of $\Gamma = W = \Gamma_0$ as functions of E_2 and E_4 for several $\delta = (E_4 - E_2)/2$. $\Gamma_0 = 10$ μeV and $V_D = 8$ μeV. (a), (d) Conductance. (b), (e) $V_{\rm out}$. (c), (f) The noise power S. (a)–(c) Three QD case and (d)–(f) five QD case.

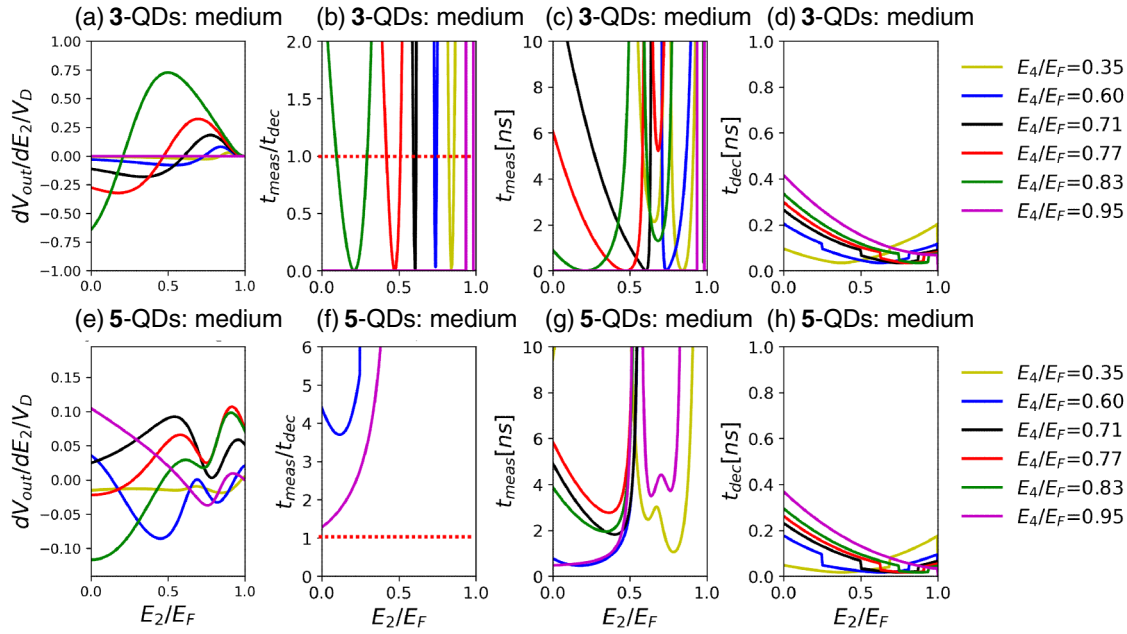

FIG. 7. The medium measurement case of $\Gamma = W = \Gamma_0$ as functions of E_2 and E_4 for several $\delta = (E_4 - E_2)/2$. $\Gamma_0 = 10\ \mu$eV and $V_D = 8\ \mu$eV. (a), (e) $\frac{dV_{\rm out}}{d(E_2-E_4)}/V_D$. (b), (f) $t_{\rm meas}/t_{\rm dec}$. (c), (g) $t_{\rm meas}$. (d), (h) $t_{\rm dec}$. (a)–(d) Three QD case and (e)–(h) five QD case. The dotted lines in (b) and (f) indicate the boundary of the effective measurement $t_{\rm meas} < t_{\rm dec}$.

of the effective measurement where the setup of $t_{\rm meas} \gtrsim t_{\rm dec}$ is meaningless because before obtaining the information of the energy levels of QD2 and QD4, the electrons dephase via the back-action of the measurement. In the three QD case [Fig. 5(b)], it is seen that the strong measurement has the narrow regions for the condition $t_{\rm meas} < t_{\rm dec}$. In the case of the five QD case [Fig. 5(f)], the effective measurement region becomes much narrower. Note that, in Figs. 5(b) and 5(c), the overlap of the small $t_{\rm meas}$ regions come from Eq. (38) where the conductance, Fig. 4(a), and the noise power, Fig. 4(c),

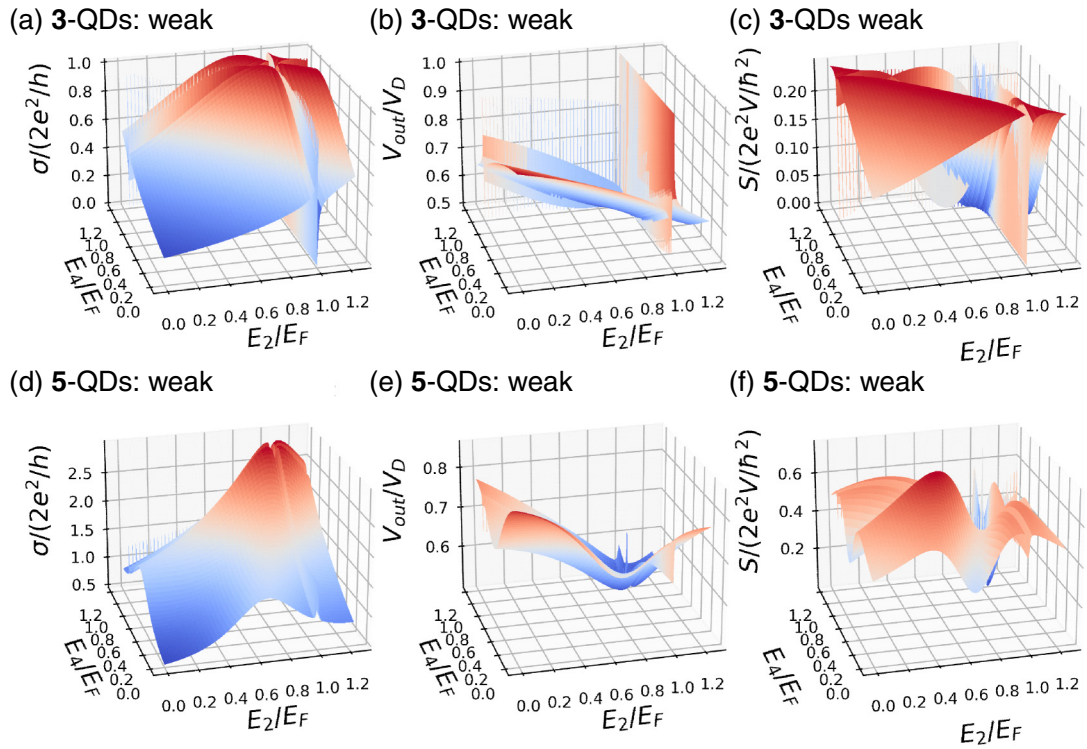

FIG. 8. The weak measurement case of $\Gamma = 2\Gamma_0$ and $W = 0.2\Gamma_0$ as functions of E_2 and E_4 for several $\delta = (E_4 - E_2)/2$. $\Gamma_0 = 10\ \mu$eV and $V_D = 8\ \mu$eV. (a), (d) Conductance. (b), (e) $V_{\rm out}$. (c), (f) The noise power S. (a)–(c) Three QD case and (d)–(f) five QD case.

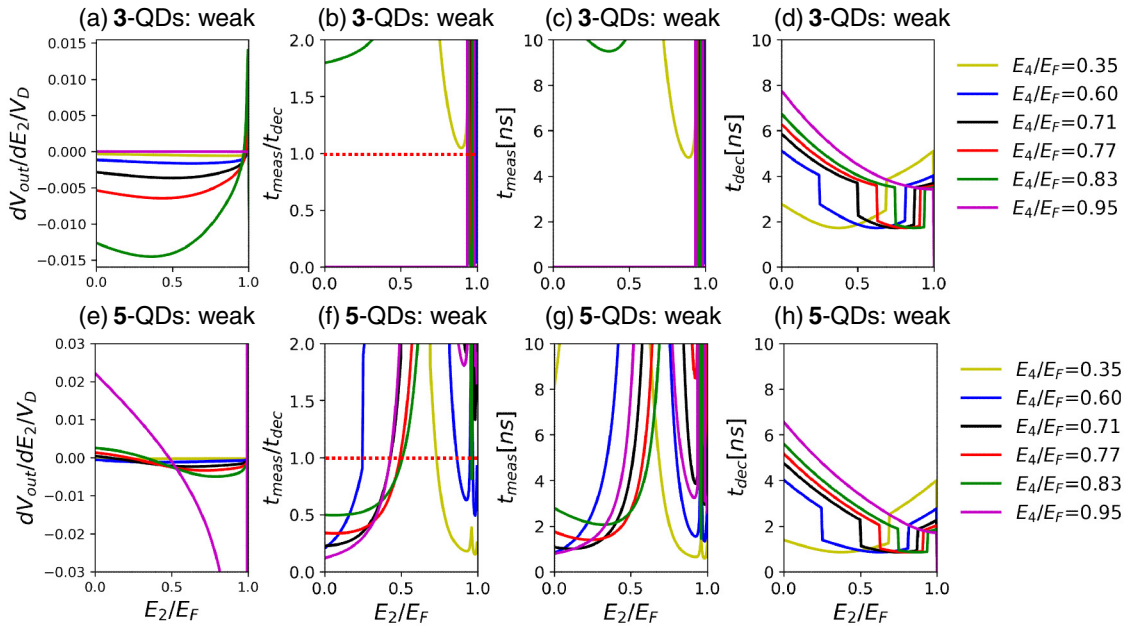

FIG. 9. The weak measurement case of $\Gamma = 2\Gamma_0$ and $W = 0.2\Gamma_0$ as functions of E_2 and E_4 for several $\delta = (E_4 - E_2)/2$. $\Gamma_0 = 10$ μeV and $V_D = 8$ μeV. (a), (e) $\frac{dV_{\rm out}}{d(E_2-E_4)}/V_D$. (b), (f) $t_{\rm meas}/t_{\rm dec}$. (c), (g) $t_{\rm meas}$. (d), (h) $t_{\rm dec}$. (a)–(d) Three QD case and (e)–(h) five QD case. The dotted lines in (b) and (f) indicate the boundary of the effective measurement $t_{\rm meas} < t_{\rm dec}$.

shows similar behavior. A larger change in $V_{\rm out}$ as the function of the difference between E_2 and E_4 is desirable. In this meaning, the strong measurement case shows the large $V_{\rm out}$ for some parameters. However, it seems that the corresponding strong measurement cases such as $E_4/E_F \leqslant 0.60$ do not hold the condition for the effective measurement condition.

Next, we consider the medium measurement case shown in Figs. 6 and 7. In case of the three QDs, it is observed that the conductance [Fig. 6(a)] decreases before the Fermi level, and increases at the Fermi level. This wall-like structure around $(E_2, E_4) = (E_F, E_F)$ of Fig. 6(a) can be partly explained by considering the zero points of the denominator of Eq. (30) given by

$$\left(1 - C^r_{23} - C^r_{34}\right)D_3 = b^*_3 - W^2\left[\frac{b^*_2}{D_2} + \frac{b^*_4}{D_4}\right] \approx 0, \quad (41)$$

where $b_i(\omega) = \omega - E_i + i\Gamma_i/2$ and $D_i = [\omega - E_i]^2 + \gamma_i^2$ ($\gamma_i = \Gamma_i/2$). The imaginary part of Eq. (41) leads to

$$\frac{\gamma_3}{W^2} = \frac{\gamma_2}{[\omega - E_2]^2 + \gamma_2^2} + \frac{\gamma_4}{[\omega - E_4]^2 + \gamma_4^2}. \quad (42)$$

For $\Gamma_3 = W$, Eq. (42) satisfies $\cos^2\theta_a + \sin^2\theta_a = 1$ if we take $\gamma_2 = \gamma_4 = 2W$ and

$$\omega - E_2 = 2W\ \tan\theta_a, \quad (43)$$

$$\omega - E_4 = 2W\ \cot\theta_a. \quad (44)$$

The real part of Eq. (41) leads to $\theta_a \approx \pi/4$ by considering $E_3 - E_2 = E_4 - E_3$. From Eqs. (43) and (44), we obtain

$$(\omega - E_2)(\omega - E_4) = 4W^2. \quad (45)$$

This equation means that the maximum current, which corresponds to the region where the denominator of Eq. (30) is around zero [Eq. (41)], is observed when E_2 and E_4 have the relation $y \propto W^2/x$ from the viewpoint at the origin of $(x, y) = (E_F, E_F)$. Compared with the three QD case, the results of the five QD case has a peak structure [Fig. 6(d)]. This is because of the complicated structure of Eq. (29). Note that the wall-like structure can also be seen in the strong measurements [Fig. 4(a)]. Because $W = 2\Gamma_0$ in the strong measurement is larger than that of the medium measurement, the wall-like structure of the strong measurement is far from the Fermi energy and close to (0,0).

Figure 6(b) shows that the large change of $V_{\rm out}$ can be seen around the wall-like structure for the three QD case, and Fig. 6(e) shows that $V_{\rm out}$ changes prominently away from the diagonal line of $E_2 = E_4$. Accordingly, Figs. 7(a) and 7(e) show the large rate of $\frac{dV_{\rm out}}{d(E_2-E_4)}/V_D$ around the middle of the Fermi surface ($E_4/E_F \approx 0.77$). Compared with Figs. 7(a) and 7(e), the three QDs have a higher amplifying rate. It is seen that $V_{\rm out}$ changes more than 0.5 V_D when E_2 changes for a fixed E_4 for the three QD case. From Figs. 7(d) and 7(h), the decoherence time of the three QD case is a little longer than that of the five QD case. Here, the abrupt change of $t_{\rm dec}$ comes from the definition of $|\omega_{01}|$ in Eq. (40) (see Appendix A and Fig. 11). When the measurement time of the three QDs [Figs. 7(b) and 7(c)] is compared with that of the strong measurement case [Figs. 5(b) and 5(c)], the effective measurement region ($t_{\rm meas} < t_{\rm dec}$) becomes larger. The comparison of $\frac{dV_{\rm out}}{d(E_2-E_4)}/V_D$ of the medium measurement case [Fig. 7(a)] with that of the strong measurement case [Fig. 5(a)] indicates that the medium measurement case will be better than the strong measurement case. In the present parameter region, there is no effective measurement region for the five QD case in the medium measurement [Fig. 7(f)]. Thus, the side-QD setup of Fig. 1(a) might be a good measurement apparatus for the energy levels of the two QDs, whereas the five QD case is meaningless in the present parameter region.

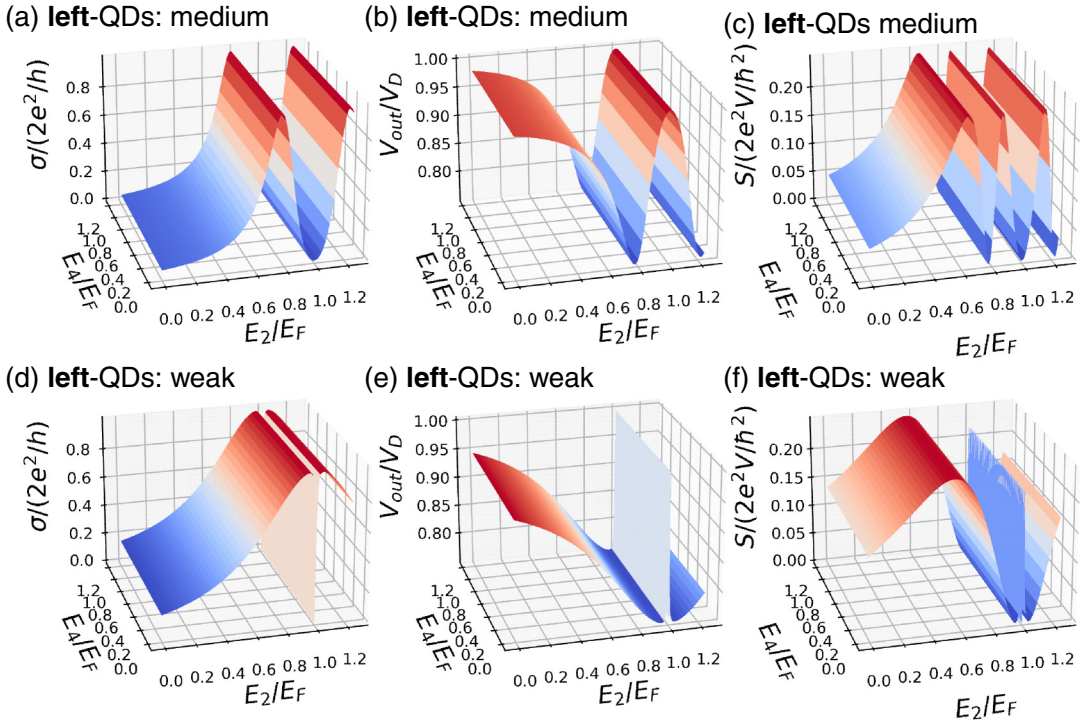

FIG. 10. The transport properties, where only the left current channel 1 is switched on. (a)–(c) For the medium measurement case ($\Gamma = W = \Gamma_0$), and (d)–(f) for the weak measurement case ($\Gamma = 2\Gamma_0$ and $W = 0.2\Gamma_0$). (a), (d) Conductance. (b), (e) $V_{\rm out}$. (c), (f) The noise power S. $\Gamma_0 = 10$ μeV and $V_D = 8$ μeV.

As seen in Fig. 3, the weak measurement case shows the Fano dip structure, and the conductances [Figs. 8(a) and 8(d)] reflect the corresponding dip structures around E_F. $V_{\rm out}$ shows sharp changes around E_F in both Figs. 8(b) and 8(e). The decoherence time of the three QD case is a little better than that of the five QD case [Figs. 9(a) and 9(e)]. In contrast, the five QD case has wider effective measurement region of $t_{\rm meas}/t_{\rm dec} < 1$, compared with the three QD case [Figs. 9(b) and 9(f)]. It is considered that the multiple current passes of the five QD case help the effective measurement in this weak measurement region. In addition, if we increase R_D more than Eq. (34), it will be possible to increase the rate $\frac{dV_{\rm out}}{d(E_2-E_4)}/V_D$ in the region of the small conductance from Eq. (35).

Figure 10 shows the case where only the current channel 1 of Fig. 1(b) is switched on. In this case, the current reflects only the energy level of the QD2. The conductance behaves differently from the numerical results mentioned above, and by comparing the current where only current 3 is switched on, we could distinguish which of the energy levels between QD2 and that of QD4 were larger.

V. DISCUSSION

As an application of the present structure, we think that our setup can be used to distinguish the two Zeeman energies. Let us estimate the concrete values of the energy difference of the Zeeman energies shown in [40] and [41]. The gradient magnetic field in [40] described the 30-mT magnetic field gradient between two QDs approximately 100 nm apart, and 0.08 mT/nm in [41], which corresponds to the 8 mT between the two QDs 100 nm apart. When we estimate the Zeeman energy for the magnetic field gradient ΔB_z (T) by $\Delta E_Z = g\mu_B \Delta B_z$ with $g_{\rm Si} = 2$ ($g_{\rm GaAs} = -0.44$) and $\mu_B = 5.789 \times 10^{-5}$ (eV/T), the energy difference of $\Delta B_z = 30$ mT corresponds to $\Delta E_Z = 3.47$ μeV for Si and $\Delta E_Z = 0.1735$ μeV for GaAs. Thus, these energy-level differences are in the same order of the present unit of the energy levels by $\Gamma_0 = 10$ μeV. Then, from the numerical results mentioned above, if we investigate detailed conditions, it will be possible to find the appropriate measurement time region. The direct comparison with experiments is the future issue.

Here, in order to remain in the linear region of Eq. (33), we have shown only the small V_D case, which is in the range of the mesoscopic experiments [1,3,7]. It is seen from Eq. (38) that, as V_D increases, the effective measurement region becomes wider. To directly connect the readout to the conventional complementary metal oxide semiconductor (CMOS) circuits [53], which is in the order of meV, we need to consider the meV region of V_D. It will be necessary to clarify the region in which the linear approximation (33) is kept by solving the nonlinear equation of Eq. (32). In any way, the numerical results change depending on the parameter regions, and to directly compare the numerical results with experiments, we need to adjust the parameters. These are near-future problems.

VI. CONCLUSION

We have theoretically investigated the three and five QD systems as the measurement system of energy levels of internal QDs by considering the additional small circuit to convert the current changes into voltage changes. We observed that depending on the coupling strength of the measurement part

and the targeted internal QDs, the conductance, noise, and output voltage change. We have also estimated the measurement time and the decoherence time, and showed the tradeoff between the measurement strength and the decoherence time. It was found that the medium measurement region of the three QDs is relatively good for the detection of the difference between two energy levels. It was also found that the three QD case shows a wide range of effective measurement regions compared with the five QD case.

ACKNOWLEDGMENTS

We are grateful to K. Ono, T. Mori, and H. Fuketa for their fruitful discussions. This work was partly supported by MEXT Quantum Leap Flagship Program (MEXT Q-LEAP) Grant No. JPMXS0118069228, Japan. The authors thank the Supercomputer Center, the Institute for Solid State Physics, and the University of Tokyo for the use of their facilities.

APPENDIX A: DEPHASING RATE

The dephasing rate described by the golden rule [52] can be calculated from the correlation function $\langle H_{\rm int}(t)H_{\rm int}(0)\rangle$, which is given by

$$\begin{aligned}
&\langle H_{\rm int}(t)H_{\rm int}(0)\rangle \\
&= \Big\langle \sum_{ij}[W_{i,i+1}d_i^\dagger(t)d_{i+1}(t) + W_{i,i+1}^* d_{i+1}^\dagger(t)d_i(t)] \\
&\quad \times [W_{j,j+1}d_j^\dagger(0)d_{j+1}(0) + W_{j,j+1}^* d_{j+1}^\dagger(0)d_j(0)]\Big\rangle \\
&= \sum_i |W_{i,i+1}|^2 \langle d_i^\dagger(t)d_i(0)\rangle\langle d_{i+1}(t)d_{i+1}^\dagger(0)\rangle \\
&\quad + |W_{i,i+1}|^2 \langle d_{i+1}^\dagger(t)d_{i+1}(0)\rangle\langle d_i(t)d_i^\dagger(0)\rangle \\
&= \sum_i |W_{i,i+1}|^2 [g_{di}^<(-t)g_{di+1}^>(t) + g_{di+1}^<(-t)g_{di}^>(t)] \\
&= \sum_i |W_{i,i+1}|^2 \iint \frac{d\epsilon}{2\pi}\frac{d\epsilon'}{2\pi}[g_{di}^<(\epsilon)g_{di+1}^>(\epsilon') \\
&\quad + g_{di+1}^<(\epsilon)g_{di}^>(\epsilon')]e^{i(\epsilon-\epsilon')t}. \qquad \text{(A1)}
\end{aligned}$$

Then, the relaxation rate is given by

$$\begin{aligned}
\Gamma_{\rm relax} &\approx \frac{1}{\hbar^2}\int_{-\infty}^{\infty} d\tau\, e^{-i\omega_{01}\tau}\langle H_{\rm int}(\tau)H_{\rm int}(0)\rangle \\
&= \sum_i \frac{|W_{i,i+1}|^2}{\hbar^2}\int \frac{d\epsilon'}{2\pi}[g_{di}^<(\epsilon'+\omega_{01})g_{di+1}^>(\epsilon') \\
&\quad + g_{di+1}^<(\epsilon'+\omega_{01})g_{di}^>(\epsilon')]. \qquad \text{(A2)}
\end{aligned}$$

The abrupt change $t_{\rm dec}$ originates from the definition of ω_{01}. For $E_2 > E_4$, $\omega_{01} = E_2 - E_4$, and we have

$$E_2 + \omega_{01} = 2E_2 - E_4,\ E_2 - \omega_{01} = E_4, \qquad \text{(A3)}$$

$$E_4 + \omega_{01} = E_2,\ E_4 - \omega_{01} = 2E_4 - E_2. \qquad \text{(A4)}$$

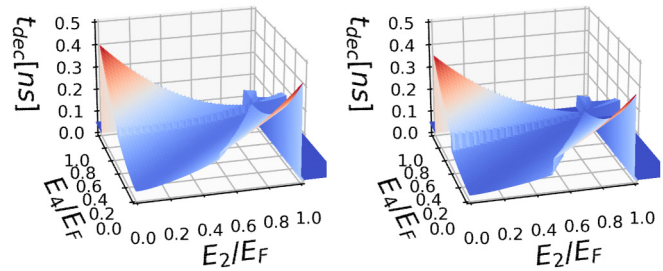

FIG. 11. 3D view of the decoherence time for the medium measurement case of $\Gamma = W = \Gamma_0$ for $\Gamma_0 = 10\ \mu$eV and $V_D = 8\ \mu$eV. (a) The three QD case and (b) the five QD case. The abrupt changes of Figs. 7 and 9 come from Eqs. (A4) and (A6).

For $E_2 < E_4$, $\omega_{01} = E_4 - E_2$, and we have

$$E_2 + \omega_{01} = E_4,\ E_2 - \omega_{01} = 2E_2 - E_4, \qquad \text{(A5)}$$

$$E_4 + \omega_{01} = 2E_4 - E_2,\ E_4 - \omega_{01} = E_2. \qquad \text{(A6)}$$

The bird's-eye views of $t_{\rm dec}$ are shown in Fig. 11.

APPENDIX B: EFFECTS OF VARIATIONS AND TEMPERATURE DEPENDENCE

It is not easy to fabricate the nanometer-sized structures, and the size variations of structures are inevitable. Here, we show a couple of numerical results regarding the effect of the variations by comparing with Figs. 7(a)–7(d). In Fig. 12, we have introduced the variations on Γ_i^α and W_{ij} by adding the randomness. The concrete values are listed in Table I. We can see the 20% variations greatly shift the appropriate measurement regions.

Figure 13 shows the conductance at finite temperature. Other than the magnitude of the conductance, the dependence of E_2 and E_4 on the conductance is similar to those for the $T = 0$ cases in the main text. The detailed temperature dependence is a future issue.

APPENDIX C: GREEN'S FUNCTIONS FOR THE QDs

In this Appendix, we show the derivation of the Green's functions based on the equation-of-motion method. From Eq. (7), we have the equations like

$$(\omega - E_1)d_1 = \sum_{k_L} V_{k_L,1}^* c_{1k_L} + \sum_{k_R} V_{k_R,1}^* c_{1k_R} + W_{12}d_2. \qquad \text{(C1)}$$

TABLE I. Concrete values used in the effect of variations.

	10% (dashed dotted)	20% (dashed dotted)	10% (dotted)	20% (dotted)
Γ_3^L/Γ_0	1.092	1.158	1.057	1.066
Γ_3^R/Γ_0	1.073	0.931	1.056	0.892
W_{32}/Γ_0	0.901	1.104	1.011	1.111
W_{34}/Γ_0	1.035	0.989	1.089	1.148

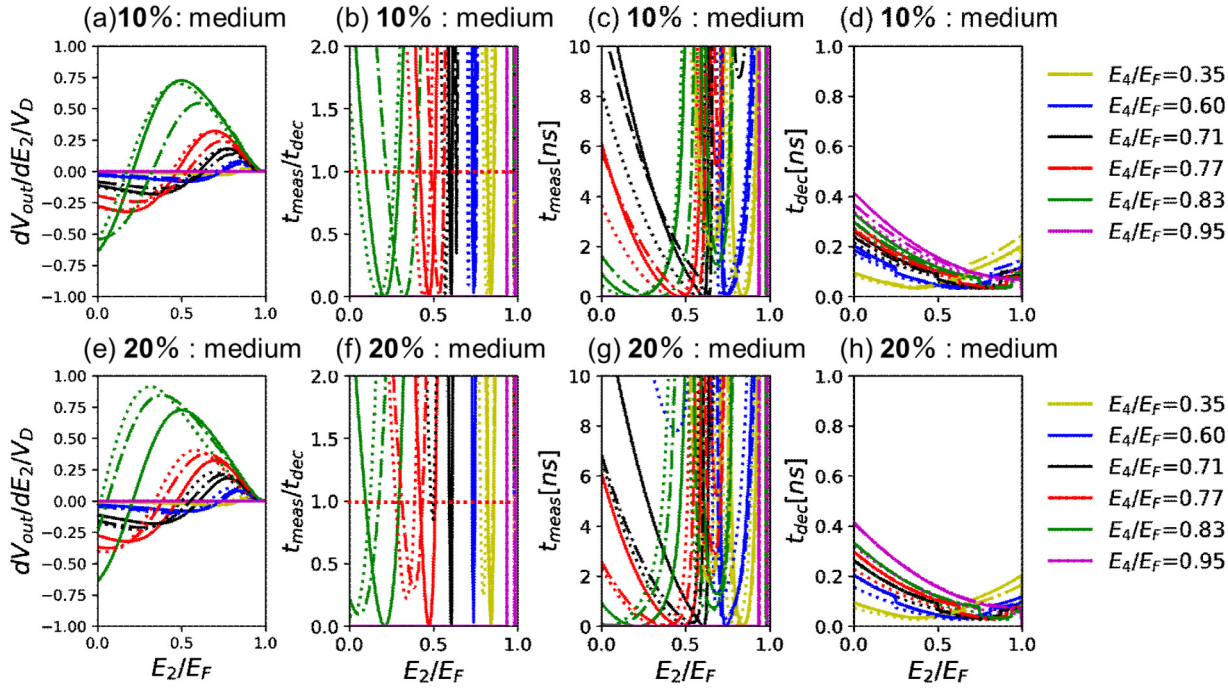

FIG. 12. The effects of the variations of Γ_i^α and W_{ij} in the medium coupling of the three QD system. We take $\Gamma_i^\alpha = \Gamma_0(1+\delta g_i^\alpha)$ and $W_{ij} = W(1+\delta w_{ij})$ $(\alpha = L, R)$ where δg_i^α and δw_{ij} are random numbers. $\Gamma_0 = 10$ μeV and $V_D = 8$ μeV. (a) 10% randomness $(-0.1 \leqslant \delta g_i^\alpha, \delta w_{ij} \leqslant 0.1)$. (b) 20% randomness $(-0.2 \leqslant \delta g_i^\alpha, \delta w_{ij} \leqslant 0.2)$. Solid lines correspond to the uniform cases [Figs. 7(a)–7(d)]. The dashed dotted and dotted lines are the results of two types of random numbers. The dashed red lines in (b) and (f) indicate the boundary of the effective measurement $t_{\rm meas} < t_{\rm dec}$.

Thus, we obtain

$$[\omega - E_1 - \Sigma_1(\omega)]G_{d_1,d_j} = W_{12}G_{d_2,d_j} + \delta_{1j}, \quad \text{(C2)}$$

$$(\omega - E_2)G_{d_2,d_j} = W_{21}G_{d_1,d_j} + W_{23}G_{d_3,d_j} + \delta_{2,j}, \quad \text{(C3)}$$

$$[\omega - E_3 - \Sigma_3(\omega)]G_{d_3,d_j} = W_{32}G_{d_2,d_j} + W_{34}G_{d_4,d_j} + \delta_{3,j}, \quad \text{(C4)}$$

$$(\omega - E_4)G_{d_4,d_j} = W_{45}G_{d_5,d_j} + W_{43}G_{d_3,d_j} + \delta_{4,j}, \quad \text{(C5)}$$

$$[\omega - E_5 - \Sigma_5(\omega)]G_{d_5,d_j} = W_{54}G_{d_4,d_j} + \delta_{5j}, \quad \text{(C6)}$$

where G_{d_i,d_j} represents $G_{d_i,d_j}(\omega)$, and

$$\Sigma_i(\omega) \equiv \sum_{k_L} \frac{|V_{k_L,i}|^2}{(\omega - E_{k_{Li}})} + \sum_{k_R} \frac{|V_{k_R,i}|^2}{(\omega - E_{k_{Ri}})}. \quad \text{(C7)}$$

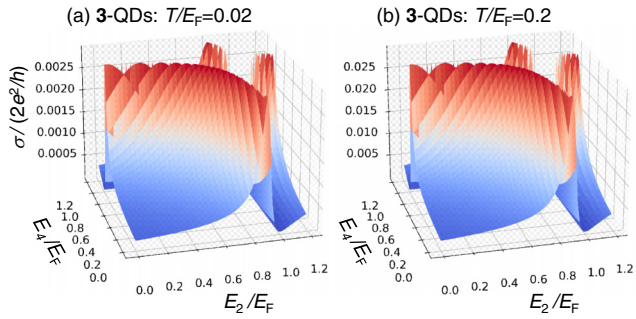

FIG. 13. The conductances at finite temperature in the medium coupling of the three QD system. (a) $T/E_F = 0.02$. (b) $T/E_F = 0.2$.

Thus, the equations between the Green's functions of the QDs are given as follows:

$$G_{d11} = W_{12}g_{d1}G_{d21} + g_{d1}, \quad \text{(C8)}$$

$$G_{d21} = C_{12}G_{d21} + W_{21}g_{d2}g_{d1} + W_{23}g_{d2}G_{d31}, \quad \text{(C9)}$$

$$G_{d22} = C_{12}G_{d22} + W_{23}g_{d2}G_{d32} + g_{d2}, \quad \text{(C10)}$$

$$G_{d23} = C_{12}G_{d23} + W_{23}g_{d2}G_{d33}, \quad \text{(C11)}$$

$$G_{d24} = C_{12}G_{d24} + W_{23}g_{d2}G_{d34}, \quad \text{(C12)}$$

$$G_{d25} = C_{12}G_{d25} + W_{23}g_{d2}G_{d35}, \quad \text{(C13)}$$

$$G_{d31} = g_{d3}(W_{32}G_{d21} + W_{34}G_{d41}), \quad \text{(C14)}$$

$$G_{d32} = g_{d3}(W_{32}G_{d22} + W_{34}G_{d42}), \quad \text{(C15)}$$

$$G_{d33} = g_{d3}(W_{32}G_{d23} + W_{34}G_{d43} + 1), \quad \text{(C16)}$$

$$G_{d34} = g_{d3}(W_{32}G_{d24} + W_{34}G_{d44}), \quad \text{(C17)}$$

$$G_{d35} = g_{d3}(W_{32}G_{d25} + W_{34}G_{d45}), \quad \text{(C18)}$$

$$G_{d41} = C_{54}G_{d41} + W_{43}g_{d4}G_{d31}, \quad \text{(C19)}$$

$$G_{d42} = C_{54}G_{d42} + W_{43}g_{d4}G_{d32}, \quad \text{(C20)}$$

$$G_{d43} = C_{54}G_{d43} + W_{43}g_{d4}G_{d33}, \quad \text{(C21)}$$

$$G_{d44} = C_{54}G_{d44} + W_{43}g_{d4}G_{d34} + g_{d4}, \quad \text{(C22)}$$

$$G_{d45} = C_{54}G_{d45} + W_{45}g_{d4}g_{d5} + W_{43}g_{d4}G_{d35}, \quad \text{(C23)}$$

$$G_{d55} = W_{54}g_{d5}G_{d45} + g_{d5}, \quad \text{(C24)}$$

where

$$g_{di}(\omega) = 1/(\omega - E_i - \Sigma_i). \quad \text{(C25)}$$

These equations can be solved by starting with the elimination of G_{d2i} and G_{d4i} $(i = 1, \ldots, 5)$ such as

$$G_{d21} = \frac{W_{21}g_{d2}g_{d1}}{(1 - C_{12})} + \frac{W_{23}g_{d2}G_{d31}}{(1 - C_{12})}, \quad \text{(C26)}$$

$$G_{d22} = \frac{W_{23}g_{d2}G_{d32}}{(1 - C_{12})} + \frac{g_{d2}}{(1 - C_{12})}, \quad \text{(C27)}$$

$$\cdots .$$

Thus, we have

$$G_{d31} = \frac{(1 - C_{54})}{\Delta_c} W_{32}W_{21}g_{d3}g_{d2}g_{d1}, \quad \text{(C28)}$$

$$G_{d32} = \frac{(1 - C_{54})}{\Delta_c} W_{32}g_{d3}g_{d2}, \quad \text{(C29)}$$

$$G_{d33} = \frac{(1 - C_{12})(1 - C_{54})}{\Delta_c} g_{d3}, \quad \text{(C30)}$$

$$G_{d34} = \frac{(1 - C_{12})}{\Delta_c} W_{34}g_{d3}g_{d4}, \quad \text{(C31)}$$

$$G_{d35} = \frac{(1 - C_{12})}{\Delta_c} W_{34}W_{45}g_{d3}g_{d4}g_{d5}. \quad \text{(C32)}$$

Here,

$$\Delta_c \equiv (1 - C_{12} - C_{32})(1 - C_{54}) - (1 - C_{12})C_{34}. \quad \text{(C33)}$$

Similarly, we have

$$G_{d11} = \frac{(1 - C_{32})(1 - C_{54}) - C_{34}}{\Delta_c} g_{d1}, \quad \text{(C34)}$$

$$G_{d55} = \frac{(1 - C_{12})(1 - C_{34}) - C_{32}}{\Delta_c} g_{d5}. \quad \text{(C35)}$$

There are the Green's functions of Eqs. (17)–(25) in the main text.

APPENDIX D: GREEN'S FUNCTION FOR THE QD-LEAD (*k*-*d*) ELEMENTS

Similar to the Green's functions of the QDs, we can derive the Green's functions of the type of $G_{d_i,k_{\alpha j}}(\omega)$ [$\equiv G_{d_i,c_{jk_\alpha}}(\omega)$ in Eq. (4) in the main text] based on the equation-of-motion method as follows:

$$[\omega - E_1 - \Sigma_1(\omega)]G_{d_1,k'_{\alpha j}} = W_{12}G_{d_2,k'_{\alpha j}} + v_{k'_{\alpha 1}}\delta_{1j}, \quad \text{(D1)}$$

$$(\omega - E_2)G_{d_2,k'_{\alpha j}} = W_{21}G_{d_1,k'_{\alpha j}} + W_{23}G_{d_3,k'_{\alpha j}}, \quad \text{(D2)}$$

$$[\omega - E_3 - \Sigma_3(\omega)]G_{d_3,k'_{\alpha j}} = W_{32}G_{d_2,k'_{\alpha j}} + W_{34}G_{d_4,k'_{\alpha j}} + v_{k'_{\alpha 3}}\delta_{3j}, \quad \text{(D3)}$$

$$(\omega - E_4)G_{d_4,k'_{\alpha j}} = W_{45}G_{d_5,k'_{\alpha j}} + W_{43}G_{d_3,k'_{\alpha j}}, \quad \text{(D4)}$$

$$[\omega - E_5 - \Sigma_5(\omega)]G_{d_5,k'_{\alpha j}} = W_{54}G_{d_4,k'_{\alpha j}} + v_{k'_{L5}}\delta_{5j}, \quad \text{(D5)}$$

where $(j = 1, 3, 5)$, and

$$v_{k'_{\alpha i}}(\omega) \equiv \frac{V^*_{k'_\alpha,i}}{(\omega - E_{k'_{\alpha i}})}. \quad \text{(D6)}$$

Hereafter we write the QD-lead Green's functions $G_{d_i,k_{\alpha j}}(\omega)$ as G_{ij}, and $v_i \equiv v_{k'_{\alpha i}}(\omega)$ for simplicity. These equations are changed into the following:

$$G_{1j} = g_{d1}(W_{12}G_{2j} + v_1\delta_{ij}), \quad \text{(D7)}$$

$$G_{2j} = g_{d2}(W_{21}G_{1j} + W_{23}G_{3j}), \quad \text{(D8)}$$

$$G_{3j} = g_{d3}(W_{32}G_{2j} + W_{34}G_{4j} + v_3\delta_{3j}), \quad \text{(D9)}$$

$$G_{4j} = g_{d4}(W_{45}G_{5j} + W_{43}G_{3j}), \quad \text{(D10)}$$

$$G_{5j} = g_{d5}(W_{54}G_{4j} + v_5). \quad \text{(D11)}$$

For the three Green's functions $A(t, t')$, $B(t, t')$, and $C(t, t')$, if $A^r(t, t') = \int dt_1 B^r(t, t_1)C^r(t_1, t')$ is held, we have the relation

$$A^<(t, t') = \int dt_1 [B^r(t, t_1)C^<(t_1, t') + B^<(t, t_1)C^a(t_1, t')]. \quad \text{(D12)}$$

When we apply this relation to Eq. (D9), we have

$$G^<_{13} - C^r_{12}G^<_{13} = W_{23}W_{12}c^r_{12}G^<_{33} + C^<_{12}G^a_{13} + W_{23}W_{12}c^<_{12}G^a_{33}, \quad \text{(D13)}$$

$$G^<_{33} - [C^r_{32} + C^r_{34}]G^<_{33} = W_{21}W_{32}c^r_{32}G^<_{13} + W_{21}W_{32}c^<_{32}G^a_{13} + W_{45}W_{34}c^r_{34}G^<_{53} + W_{45}W_{34}c^<_{34}G^a_{53} + [C^<_{32} + C^<_{34}]G^a_{33} + [g_{d3}v_3]^<, \quad \text{(D14)}$$

$$G^<_{53} - C^r_{54}G^<_{53} = W_{43}W_{54}c^r_{54}G^<_{33} + C^<_{54}G^a_{53} + W_{43}W_{54}c^<_{54}G^a_{33}, \quad \text{(D15)}$$

where

$$c^{r,a}_{ij} = (g_{di}g_{dj})^{r,a} = g^{r,a}_{di}g^{r,a}_{dj}, \quad \text{(D16)}$$

$$c^<_{ij} = (g_{di}g_{dj})^< = g^r_{di}g^<_{dj} + g^<_{di}g^a_{dj}, \quad \text{(D17)}$$

$$C^{r,a}_{ij} = |W_{ij}|^2 c^{r,a}_{ij}, \quad \text{(D18)}$$

$$C^<_{ij} = |W_{ij}|^2 c^<_{ij}. \quad \text{(D19)}$$

Here, we use the expressions of Eqs. (17)–(25). For example,

$$C^<_{12}G^a_{13} + W_{23}W_{12}c^<_{12}G^a_{33} = \frac{(1 - C^a_{54})}{\Delta^a_c} W_{23}W_{12}c^<_{12}g^a_{d3}v^a_3, \quad \text{(D20)}$$

$$W_{21}W_{32}c^<_{32}G^a_{13} + C^<_{32}G^a_{33} = \frac{(1 - C^a_{54})}{\Delta^a_c} C^<_{32}g^a_{d3}v^a_3, \quad \text{(D21)}$$

$$C^<_{54}G^a_{53} + W_{43}W_{54}c^<_{54}G^a_{33} = \frac{(1 - C^a_{12})}{\Delta^a_c} C^<_{34}g^a_{d3}v^a_3. \quad \text{(D22)}$$

Then, we have

$$G^<_{13} = W_{23}W_{12}\frac{c^r_{12}G^<_{33} + c^<_{12}g^a_{133}}{\left(1-C^r_{12}\right)}, \tag{D23}$$

$$G^<_{53} = W_{43}W_{54}\frac{c^r_{54}G^<_{33} + c^<_{54}g^a_{533}}{\left(1-C^r_{54}\right)}, \tag{D24}$$

where

$$g^a_{133} = \frac{\left(1-C^a_{54}\right)}{\Delta^a_c}g^a_{d3}v^a_3, \tag{D25}$$

$$g^a_{533} = \frac{\left(1-C^a_{12}\right)}{\Delta^a_c}g^a_{d3}. \tag{D26}$$

Thus, we have

$$\begin{aligned}
G^<_{33} &= \left|1-C^r_{54}\right|^2\frac{\left[C^r_{32}C^<_{12}+C^<_{32}\left(1-C^r_{12}\right)\right]g^a_{d3}v^a_3-\left(1-C^r_{12}\right)C^a_{32}[g_{d3}v_3]^<}{\left|\Delta^r_c\right|^2}\\
&\quad+\left|1-C^r_{12}\right|^2\frac{\left[C^r_{34}C^<_{54}+C^<_{34}\left(1-C^r_{54}\right)\right]g^a_{d3}v^a_3-\left(1-C^r_{54}\right)C^a_{34}[g_{d3}v_3]^<}{\left|\Delta^r_c\right|^2}+\left|1-C^r_{54}\right|^2\left|1-C^r_{12}\right|^2\frac{[g_{d3}v_3]^<}{\left|\Delta^r_c\right|^2}\\
&= \left|1-C^r_{54}\right|^2\frac{|W_{23}|^2|W_{12}|^2|g_{d2}|^2|g_{d3}|^2\left(g^<_{d1}v^a_3+g^r_{d1}v^<_3\right)+|W_{32}|^2\left|g^r_{d3}\right|^2\left[g^<_{d2}v^a_3-g^a_{d2}v^<_3\right]}{\left|\Delta^r_c\right|^2}\\
&\quad+|1-C^r_{12}|^2\frac{|W_{43}|^2|W_{54}|^2|g_{d4}|^2|g_{d3}|^2\left(g^<_{d5}v^a_3+g^r_{d5}v^<_3\right)+|W_{34}|^2\left|g^r_{d3}\right|^2\left[g^<_{d4}v^a_3-g^a_{d4}v^<_3\right]}{|\Delta^r_c|^2}\\
&\quad+\left|1-C^r_{54}\right|^2\left|1-C^r_{12}\right|^2\frac{\left[g^r_3v^<_3+g^<_3v^a_3\right]}{\left|\Delta^r_c\right|^2}.
\end{aligned} \tag{D27}$$

Next, we consider the derivation of G_{55} from Eq. (D11):

$$G^<_{15}-C^r_{12}G^<_{15} = C^<_{12}G^a_{15}+W_{23}W_{12}c^r_{12}G^<_{35}+W_{23}W_{12}c^<_{12}G^a_{35}, \tag{D28}$$

$$\begin{aligned}
G^<_{35}-\left[C^r_{32}+C^r_{34}\right]G^<_{35} &= \left[C^<_{32}+C^<_{34}\right]G^a_{35}+W_{21}W_{32}c^r_{32}G^<_{15}\\
&\quad+W_{21}W_{32}c^<_{32}G^a_{15}+W_{45}W_{34}c^r_{34}G^<_{55}\\
&\quad+W_{45}W_{34}c^<_{34}G^a_{55},
\end{aligned} \tag{D29}$$

$$\begin{aligned}
G^<_{55}-C^r_{54}G^<_{55} &= C^<_{54}G^a_{55}+W_{43}W_{54}c^r_{54}G^<_{35}\\
&\quad+W_{43}W_{54}c^<_{54}G^a_{35}+(g_{d5}v_5)^<.
\end{aligned} \tag{D30}$$

Equation (D28) is changed to

$$G^<_{15} = \frac{W_{23}W_{12}c^r_{12}}{\left(1-C^r_{12}\right)}G^<_{35}+\frac{C^<_{12}}{\left(1-C^r_{12}\right)}g^a_{135}, \tag{D31}$$

where

$$g^a_{135} \equiv \frac{W_{23}W_{12}W_{45}W_{34}}{|W_{12}|^2}\frac{c^a_{34}}{\Delta^a_c}(g_{d5}v_5)^a. \tag{D32}$$

Equation (D29) is changed to

$$\begin{aligned}
&\frac{\left(1-C^r_{34}\right)\left(1-C^r_{12}\right)-C^r_{32}}{\left(1-C^r_{12}\right)}G^<_{35}\\
&\quad= W_{45}W_{34}c^r_{34}G^<_{55}+\left[C^<_{32}+\frac{C^r_{32}C^<_{12}}{\left(1-C^r_{12}\right)}\right]h^a_{135}+C^<_{34}g^a_{535},
\end{aligned}$$

where

$$h^a_{135} \equiv \frac{W_{45}W_{34}c^a_{34}}{\Delta^a_c}(g_{d5}v_5)^a, \tag{D33}$$

$$g^a_{535} \equiv \frac{W_{45}W_{34}\left[1-C^a_{12}-C^a_{32}\right]}{|W_{34}|^2\Delta^a_c}g_{d5}v^a_5. \tag{D34}$$

Equation (D30) is changed to

$$\left(1-C^r_{54}\right)G^<_{55} = W_{43}W_{54}c^r_{54}G^<_{35}+C^<_{54}h^a_{535}+(g_{d5}v_5)^<, \tag{D35}$$

where

$$h^a_{535} \equiv \frac{1-C^a_{12}-C^a_{32}}{\Delta^a_c}(g_{d5}v_5)^a. \tag{D36}$$

Thus, we have

$$\begin{aligned}
G^<_{55} &= \frac{|W_{32}W_{34}W_{54}|^2}{\left|\Delta^r_c\right|^2}|g_{d3}|^2|g_{d4}|^2|g_{d5}|^2\left\{|W_{12}|^2|g_{d2}|^2\left(g^r_{d1}v^<_5+g^<_{d1}v^a_5\right)+\left(g^<_{d2}v^a_5-g^a_{d2}v^<_5\right)\right\}\\
&\quad+|W_{34}W_{54}|^2\frac{\left|1-C^r_{12}\right|^2}{\left|\Delta^r_c\right|^2}|g_{d4}|^2|g_{d5}|^2\left[g^r_{d3}v^<_5+g^<_{d3}v^a_5\right]+|W_{54}|^2\frac{\left|1-C^r_{12}-C^r_{32}\right|^2}{\left|\Delta^r_c\right|^2}|g_{d5}|^2\left(g^<_{d4}v^a_5-g^a_{d4}v^<_5\right)\\
&\quad+\frac{\left|\left(1-C^r_{34}\right)\left(1-C^r_{12}\right)-C^r_{32}\right|^2}{\left|\Delta^r_c\right|^2}\left(g^r_{d5}v^<_5+g^<_{d5}v^a_5\right).
\end{aligned} \tag{D37}$$

By exchanging "(1,2)" with "(5,4)", we obtain the expression of $G_{11}(\omega)$.

Finally, we input the following relations into the above equations:

$$g^r_{di}(\omega) = \frac{a_i(\omega) - i\gamma_i}{D_i(\omega)}, \tag{D38}$$

$$a_i(\omega) = \omega - E_{di} - \Lambda_i(\omega),\ D_i = a_i^2 + \gamma_i^2, \tag{D39}$$

$$g^<_{di}(\omega) = iF(\omega)/D_i(\omega), \tag{D40}$$

$$F_i = \Gamma_{iL} f_{iL}(\omega) + \Gamma_{iR} f_{iR}(\omega). \tag{D41}$$

As explained in the main text, from the assumption that the total current is conserved between the source (left electrode) and drain (right electrode) such as $I_L = -I_R$, we can express the current $I = (I_L + I_L)/2 = (I_L - I_R)/2 = \sum_{i=1,3,5}(I_{iL} - I_{iR})/2$. This means that each current element can be symmetrized to $I_i = (I_{iL} + I_{iL})/2 = (I_{iL} - I_{iR})/2$ in the formulation, and we have

$$v^r_L - v^r_R \Rightarrow \frac{1}{2\pi}(\Gamma^L - \Gamma^R)\left[P\frac{1}{\omega - E_k} - i\pi\delta(\omega - E_k)\right]. \tag{D42}$$

Then, we can use the equations as follows:

$$g^r_{d1}v^<_1 + g^<_{d1}v^a_1 + \left(g^r_{d1}v^<_1 + g^<_{d1}v^a_1\right)^* \Rightarrow \frac{1}{D_1(\omega)}\Gamma^R_1\Gamma^L_1[f_{1L}(\omega) - f_{1R}(\omega)], \tag{D43}$$

$$\begin{aligned} g^r_{d1}v^<_5 + g^<_{d1}v^a_5 + \left(g^r_{d1}v^<_5 + g^<_{d1}v^a_5\right)^* \Rightarrow \frac{1}{D_1}\{&[\Gamma_{1L} + \Gamma_{1R}][\Gamma_{5L}f_{5L}(\omega) - \Gamma_{5R}f_{5R}(\omega)] \\ &- [\Gamma_{5L} - \Gamma_{5R}][\Gamma_{1L}f_{1L}(\omega) + \Gamma_{1R}f_{1R}(\omega)]\}\delta(\omega - E_{5k}), \end{aligned} \tag{D44}$$

$$g^<_{d2}v^a_5 - g^a_{d2}v^<_5 + \left(g^<_{d2}v^a_5 - g^a_{d2}v^<_5\right)^* \Rightarrow \pi\{\Gamma_{5L}[f_{5L}(E_2) - f(E_2)] - \Gamma_{5R}[f_{5R}(E_2) - f(E_2)]\}\delta(E_2 - E_{5k}). \tag{D45}$$

Thus, the current (29) is given by calculating from $I = I_1 + I_3 + I_5$, where

$$I_i = \frac{e}{\hbar}\sum_k \int \frac{d\omega}{2\pi}\{V_{ki}G^<_{ii} + V^*_{ki}(G^<_{ii})^*\}. \tag{D46}$$

Concretely, we have

$$\begin{aligned} I_3 =\ & \frac{e}{h}\int d\omega \Bigg\{ \frac{\left|1 - C^r_{54}\right|^2|W_{23}|^2|W_{12}|^2}{|\Delta^r_c|^2 D_1D_2D_3}\{[\Gamma_{1L} + \Gamma_{1R}][\Gamma_{3L}f_{3L}(\omega) - \Gamma_{3R}f_{3R}(\omega)] - [\Gamma_{3L} - \Gamma_{3R}][\Gamma_{1L}f_{1L}(\omega) + \Gamma_{1R}f_{1R}(\omega)]\} \\ &+ \frac{\left|1 - C^r_{12}\right|^2|W_{43}|^2|W_{54}|^2}{\left|\Delta^r_c\right|^2 D_3D_4D_5}\{[\Gamma_{5L} + \Gamma_{5R}][\Gamma_{3L}f_{3L}(\omega) - \Gamma_{3R}f_{3R}(\omega)] - [\Gamma_{3L} - \Gamma_{3R}][\Gamma_{5L}f_{5L}(\omega) + \Gamma_{5R}f_{5R}(\omega)]\} \\ &+ \frac{\left|1 - C^r_{54}\right|^2\left|1 - C^r_{12}\right|^2}{\left|\Delta^r_c\right|^2 D_1(\omega)}\Gamma^R_3\Gamma^L_3[f_{3L}(\omega) - f_{3R}(\omega)]\Bigg\} \\ \Rightarrow\ & \frac{e}{h}\int d\omega\left\{\frac{\left|1 - C^r_{54}\right|^2|W_{23}|^2|W_{12}|^2}{\left|\Delta^r_c\right|^2 D_1D_2D_3}F_{a31} + \frac{\left|1 - C^r_{12}\right|^2|W_{43}|^2|W_{54}|^2}{\left|\Delta^r_c\right|^2 D_3D_4D_5}F_{a35} + \frac{\left|1 - C^r_{54}\right|^2\left|1 - C^r_{12}\right|^2}{\left|\Delta^r_c\right|^2 D_3}F_{33}\right\}. \end{aligned} \tag{D47}$$

The current I_1 is given by

$$\begin{aligned} I_1 =\ & \frac{e}{h}\int d\omega \Bigg\{ \frac{|W_{34}W_{32}W_{12}W_{54}|^2}{\left|\Delta^r_c\right|^2 D_1D_2D_3D_4D_5}\{[\Gamma_{5L} + \Gamma_{5R}][\Gamma_{1L}f_{1L}(\omega) - \Gamma_{1R}f_{1R}(\omega)] - [\Gamma_{1L} - \Gamma_{1R}][\Gamma_{5L}f_{5L}(\omega) + \Gamma_{5R}f_{5R}(\omega)]\} \\ &+ \frac{|W_{32}W_{12}|^2|1 - C^r_{54}|^2}{\left|\Delta^r_c\right|^2 D_1D_2D_3}\{[\Gamma_{3L} + \Gamma_{3R}][\Gamma_{1L}f_{1L}(\omega) - \Gamma_{1R}f_{1R}(\omega)] - [\Gamma_{1L} - \Gamma_{1R}][\Gamma_{3L}f_{3L}(\omega) + \Gamma_{3R}f_{3R}(\omega)]\} \\ &+ \frac{\left|\left(1 - C^r_{32}\right)\left(1 - C^r_{54}\right) - C^r_{34}\right|^2}{\left|\Delta^r_c\right|^2 D_1}\Gamma^R_1\Gamma^L_1[f_{1L}(\omega) - f_{1R}(\omega)]\Bigg\} \\ \Rightarrow\ & \frac{e}{h}\int d\omega\left\{\frac{|W_{34}W_{32}W_{12}W_{54}|^2}{\left|\Delta^r_c\right|^2 D_1D_2D_3D_4D_5}F_{b15} + \frac{|W_{32}W_{12}|^2\left|1 - C^r_{54}\right|^2}{\left|\Delta^r_c\right|^2 D_1D_2D_3}F_{b13} + \frac{\left|\left(1 - C^r_{32}\right)\left(1 - C^r_{54}\right) - C^r_{34}\right|^2}{\left|\Delta^r_c\right|^2}\frac{F_{11}}{D_1}\right\}. \end{aligned} \tag{D48}$$

I_5 is obtained by replacing $1 \leftrightarrow 5$ and $2 \leftrightarrow 4$. We have also defined

$$F_{a31} = [\Gamma_{1L} + \Gamma_{1R}][\Gamma_{3L} f_{3L}(\omega) - \Gamma_{3R} f_{3R}(\omega)] - [\Gamma_{3L} - \Gamma_{3R}][\Gamma_{1L} f_{1L}(\omega) + \Gamma_{1R} f_{1R}(\omega)], \tag{D49}$$

$$F_{a35} = [\Gamma_{5L} + \Gamma_{5R}][\Gamma_{3L} f_{3L}(\omega) - \Gamma_{3R} f_{3R}(\omega)] - [\Gamma_{3L} - \Gamma_{3R}][\Gamma_{5L} f_{5L}(\omega) + \Gamma_{5R} f_{5R}(\omega)], \tag{D50}$$

$$F_{b15} = [\Gamma_{5L} + \Gamma_{5R}][\Gamma_{1L} f_{1L}(\omega) - \Gamma_{1R} f_{1R}(\omega)] - [\Gamma_{1L} - \Gamma_{1R}][\Gamma_{5L} f_{5L}(\omega) + \Gamma_{5R} f_{5R}(\omega)], \tag{D51}$$

$$F_{b13} = [\Gamma_{3L} + \Gamma_{3R}][\Gamma_{1L} f_{1L}(\omega) - \Gamma_{1R} f_{1R}(\omega)] - [\Gamma_{1L} - \Gamma_{1R}][\Gamma_{3L} f_{3L}(\omega) + \Gamma_{3R} f_{3R}(\omega)]. \tag{D52}$$

In the main text, we use

$$F_{ii} = \Gamma_i^R \Gamma_i^L [f_{iL}(\omega) - f_{iR}(\omega)], \tag{D53}$$

$$F_{12345} \equiv F_{b15} + F_{b51}, \tag{D54}$$

$$F_{123} \equiv F_{a31} + F_{b13}, \tag{D55}$$

$$F_{345} \equiv F_{a35} + F_{b53}. \tag{D56}$$

[1] E. Buks, R. Schuster, M. Heiblum, D. Mahalu, and V. Umansky, Nature (London) **391**, 871 (1998).
[2] T. Fujisawa, D. G. Austing, Y. Tokura, Y. Hirayama, and S. Tarucha, Nature (London) **419**, 278 (2002).
[3] G. Shinkai, T. Hayashi, T. Ota, and T. Fujisawa, Phys. Rev. Lett. **103**, 056802 (2009).
[4] T. Nakajima, A. Noiri, K. Kawasaki, J. Yoneda, P. Stano, S. Amaha, T. Otsuka, K. Takeda, M. R. Delbecq, G. Allison, A. Ludwig, A. D. Wieck, D. Loss, and S. Tarucha, Phys. Rev. X **10**, 011060 (2020).
[5] M. Sato, H. Aikawa, K. Kobayashi, S. Katsumoto, and Y. Iye, Phys. Rev. Lett. **95**, 066801 (2005).
[6] A. A. Clerk, X. Waintal, and P. W. Brouwer, Phys. Rev. Lett. **86**, 4636 (2001).
[7] A. C. Johnson, C. M. Marcus, M. P. Hanson, and A. C. Gossard, Phys. Rev. Lett. **93**, 106803 (2004).
[8] M. Kroner, A. O. Govorov, S. Remi, B. Biedermann, S. Seidl, A. Badolato, P. M. Petroff, W. Zhang, R. Barbour, B. D. Gerardot, R. J. Warburton, and K. Karrai, Nature (London) **451**, 311 (2008).
[9] S. Sasaki, H. Tamura, T. Akazaki, and T. Fujisawa, Phys. Rev. Lett. **103**, 266806 (2009).
[10] A. W. Rushforth, C. G. Smith, I. Farrer, D. A. Ritchie, G. A. C. Jones, D. Anderson, and M. Pepper, Phys. Rev. B **73**, 081305(R) (2006).
[11] T. Hensgens, T. Fujita, L. Janssen, Xiao Li, C. J. Van Diepen, C. Reichl, W. Wegscheider, S. Das Sarma, and L. M. K. Vandersypen, Nature (London) **548**, 70 (2017).
[12] A. R. Mills, M. M. Feldman, C. Monical, P. J. Lewis, K. W. Larson, A. M. Mounce, and J. R. Petta, Appl. Phys. Lett. **115**, 113501 (2019).
[13] F. Fedele, A. Chatterjee, S. Fallahi, G. C. Gardner, M. J. Manfra, and F. Kuemmeth, PRX Quantum **2**, 040306 (2021).
[14] W. Ha, S. D. Ha, M. D. Choi, Y. Tang, A. E. Schmitz, M. P. Levendorf, K. Lee, J. M. Chappell, T. S. Adams, D. R. Hulbert, E. Acuna, R. S. Noah, J. W. Matten, M. P. Jura, J. A. Wright, M. T. Rakher, and M. G. Borselli, Nano Lett. **22**, 1443 (2022).
[15] A. A. Clerk, M. H. Devoret, S. M. Girvin, F. Marquardt, and R. J. Schoelkopf, Rev. Mod. Phys. **82**, 1155 (2010).
[16] W. H. Zurek, Rev. Mod. Phys. **75**, 715 (2003).
[17] P. Bethke, R. P. G. McNeil, J. Ritzmann, T. Botzem, A. Ludwig, A. D. Wieck, and H. Bluhm, Phys. Rev. Lett. **125**, 047701 (2020).
[18] K. Horibe, T. Kodera, and S. Oda, Appl. Phys. Lett. **106**, 053119 (2015).
[19] Y. Pan, J. Zhang, E. Cohen, C.-W. Wu, P.-X. Chen, and N. Davidson, Nat. Phys. **16**, 1206 (2020).
[20] T.-S. Kim and S. Hershfield, Phys. Rev. B **63**, 245326 (2001).
[21] K. Kang, S. Y. Cho, J.-J. Kim, and S.-C. Shin, Phys. Rev. B **63**, 113304 (2001).
[22] P. Durganandini, Phys. Rev. B **74**, 155309 (2006).
[23] P. S. Cornaglia and D. R. Grempel, Phys. Rev. B **71**, 075305 (2005).
[24] K. Takahashi and T. Aono, Phys. Rev. B **74**, 041311(R) (2006).
[25] K. Takahashi and T. Aono, Phys. Rev. E **75**, 026207 (2007).
[26] T. Tanamoto and Y. Nishi, Phys. Rev. B **76**, 155319 (2007).
[27] W. Izumida and O. Sakai, Phys. Rev. B **62**, 10260 (2000).
[28] P. Coleman, Phys. Rev. B **35**, 5072 (1987).
[29] *Many-Body Physics: From Kondo to Hubbard*, edited by E. Pavarini, E. Koch, and P. Coleman (Forschungszentrum Julich, Julich, 2015), Chap. 1, 1.1–1.34.
[30] D. M. Newns and N. Read, Adv. Phys. **36**, 799 (1987).
[31] T. V. Shahbazyan and M. E. Raikh, Phys. Rev. B **49**, 17123 (1994).
[32] R. H. Dicke, Phys. Rev. **89**, 472 (1953).
[33] T. Brandes, Phys. Rep. **408**, 315 (2005).
[34] P. A. Orellana, G. A. Lara, and E. V. Anda, Phys. Rev. B **74**, 193315 (2006).
[35] E. Vernek, P. A. Orellana, and S. E. Ulloa, Phys. Rev. B **82**, 165304 (2010).
[36] P. Trocha, and J. Barnaś, Phys. Rev. B **78**, 075424 (2008).
[37] Q. Wang, H. Xie, Y.-H. Nie, and W. Ren, Phys. Rev. B **87**, 075102 (2013).

[38] S. Głodzik, K. P. Wójcik, I. Weymann, and T. Domański, Phys. Rev. B **95**, 125419 (2017).
[39] I. A. González, M. Pacheco, A. M. Calle, E. C. Siqueira, and P. A. Orellana, Sci. Rep. **11**, 3941 (2021); S. Doniach, Physica B+C **91**, 231 (1977).
[40] K. Takeda, J. Kamioka, T. Otsuka, J. Yoneda, T. Nakajima, M. R. Delbecq, S. Amaha, G. Allison, T. Kodera, S. Oda, and S. Tarucha, Sci. Adv. **2**, e1600694 (2016).
[41] T. Struck, A. Hollmann, F. Schauer, O. Fedorets, A. Schmidbauer, K. Sawano, H. Riemann, N. V. Abrosimov, Ł. Cywiński, D. Bougeard, and L. R. Schreiber, npj Quantum Inf. **6**, 40 (2020).
[42] G. P. Lansbergen *et al.*, Nat. Phys. **4**, 656 (2008).
[43] T. Tanamoto and K. Ono, AIP Adv. **11**, 045004 (2021).
[44] Y. Meir, N. S. Wingreen, and P. A. Lee, Phys. Rev. Lett. **66**, 3048 (1991).
[45] A. P. Jauho, N. S. Wingreen, and Y. Meir, Phys. Rev. B **50**, 5528 (1994).
[46] R. M. Potok, I. G. Rau, Hadas Shtrikman, Yuval Oreg, and D. Goldhaber-Gordon, Nature (London) **446**, 167 (2007).
[47] L. J. Zhu, S. H. Nie, P. Xiong, P. Schlottmann, and J. H. Zhao, Nat. Commun. **7**, 10817 (2016).
[48] K. Kobayashi and M. Hashisaka, J. Phys. Soc. Jpn. **90**, 102001 (2021).
[49] Ya. M. Blanter, M. Bŭttiker, Phys. Rep. **336**, 1 (2000).
[50] Y. Makhlin, G. Schön, and A. Shnirman, Rev. Mod. Phys. **73**, 357 (2001).
[51] H.-A. Engel and D. Loss, Phys. Rev. Lett. **86**, 4648 (2001).
[52] R. J. Schoelkopf, A. A. Clerk, S. M. Girvin, K. W. Lehnert, and M. H. Devoret, *Quantum Noise in Mesoscopic Physics* (Springer, Berlin, 2003), pp. 175–203.
[53] T. Tanamoto and K. Ono, Appl. Phys. Lett. **119**, 174002 (2021).